Pontifícia Universidade Católica
do Rio de Janeiro

Miguel Ángel Ampuero Suárez

Topology optimization for eigenvalue problems using polygonal finite elements

Dissertação de Mestrado

Thesis presented to the programa de Pós-Graduação em Engenharia Mecânica of the Departamento de Engenharia Mecânica do Centro Técnico Científico da PUC-Rio, as partial fulfillment of the requirements for the degree of Mestre em Engenharia Mecânica.

Advisor: Prof. Ivan Fabio Mota de Menezes
Co-Advisor: Prof. Anderson Pereira

Rio de Janeiro
April 2016

Miguel Ángel Ampuero Suárez

Topology optimization for eigenvalue problems using polygonal finite elements

Thesis presented to the programa de Pós-Graduação em Engenharia Mecânica of the Departamento de Engenharia Mecânica do Centro Técnico Científico da PUC-Rio, as partial fulfillment of the requirements for the degree of Mestre em Engenharia Mecânica.

Prof. Ivan Fabio Mota de Menezes
Advisor
Departamento de Engenharia Mecânica – PUC-Rio

Prof. Anderson Pereira
Co-Advisor
Departamento de Estruturas e Fundações – UERJ

Prof. Carlos Alberto de Almeida
Departamento de Engenharia Mecânica – PUC-Rio

Prof. Rodrigo Bird Burgos
Departamento de Estruturas e Fundações – UERJ

Prof. Márcio da Silveira Carvalho
Coordinator of the Centro Técnico Científico da PUC-Rio

Rio de Janeiro, April 7th ,2016.

Miguel Ángel Ampuero Suárez

The autor graduated from Universidad Nacional de Ingeniería UNI, Lima, Perú in Mechanical Electrical Engineering in 2010. Title Professional Mechanical Electrician engineer by Colegio de Ingenieros del Perú in 2013. Lima, Perú.

Bibliographic data

Ampuero Suárez, Miguel Ángel

Topology optimization for eigenvalue problems using polygonal finite elements / Miguel Ángel Ampuero Suárez; advisor: Ivan Fabio Mota de Menezes ; co-advisor: Anderson Pereira. – 2016.

91 f. : il. color. ; 30 cm

Dissertação (mestrado) – Pontifícia Universidade Católica do Rio de Janeiro, Departamento de Engenharia Mecânica, 2016.

Inclui bibliografia

1. Engenharia mecânica – Teses. 2. Otimização topológica. 3. Frequências naturais de vibração. 4. Carga crítica linearizada. 5. Problema de autovalor. 6. Elementos finitos poligonais. I. Menezes, Ivan Fabio Mota de. II. Pereira, Anderson. III. Pontifícia Universidade Católica do Rio de Janeiro. Departamento de Engenharia Mecânica. IV. Título.

CDD: 621

To my parents Paulino and Juana, my brothers Edwin and Jenifer,
for their supports and motivations.

Acknowledgments

This thesis has made possible due to the guidance of Ivan Menezes, his support, valuable comments, suggestions and provisions allowed the completion and success of this study.

Anderson Pereira for his time in checking this manuscript, comments that accelerated the development of this work and his technical support.

My classmates and my friends.

PUC-Rio, its teachers, support and administrative team.

CAPES, for their financial support.

Last but not least, to GOD, the source of understanding.

Abstract

Ampuero Suárez, Miguel Ángel; Mota de Menezes, Ivan Fabio (Advisor); Pereira, Anderson (Co-Advisor). **Topology optimization for eigenvalue problems using polygonal finite elements**. Rio de Janeiro, 2016. 91p. MSc. Dissertation - Departamento de Engenharia Mecânica, Pontifícia Universidade Católica do Rio de Janeiro.

In this work, we present some applications of topology optimization for eigenvalue problems where the main goal is to maximize a specified eigenvalue, such as a natural frequency or a linearized buckling load using polygonal finite elements in arbitrary two-dimensional domains. Topology optimization has commonly been used to minimize the compliance of structures subjected to volume constraints. The idea is to distribute a certain amount of material in a given design domain subjected to a set of loads and boundary conditions such that to maximize its stiffness. In this work, the objective is to obtain the optimal material distribution in order to maximize the fundamental natural frequency (*e.g.* to keep it away from an external excitation frequency) or to maximize the lowest critical buckling load (*e.g.* to ensure a higher level of stability of the structures). We employ unstructured polygonal meshes constructed using Voronoi tessellations for the solution of the structural topology optimization problems. The design variables, *i.e.* material densities, used in the optimization scheme, are associated with each polygonal element in the mesh. We present several topology optimization examples for both eigenfrequency and buckling problems in order to demonstrate the functionality and applicability of the proposed methodology.

.

Keywords

Topology optimization; natural frequencies; linearized buckling; eigenvalue problem; polygonal finite elements.

Resumo

Ampuero Suárez, Miguel Ángel; Mota de Menezes, Ivan Fabio (orientador); Pereira, Anderson (coorientador). **Otimização topológica para problemas de autovalor usando elementos finitos poligonais.** Rio de Janeiro, 2016. 91p. Dissertação de Mestrado - Departamento de Engenharia Mecânica, Pontifícia Universidade Católica do Rio de Janeiro.

Neste trabalho, são apresentadas algumas aplicações da otimização topológica para problemas de autovalor onde o principal objetivo é maximizar um determinado autovalor, como por exemplo uma frequência natural de vibração ou uma carga crítica linearizada, usando elementos finitos poligonais em domínios bidimensionais arbitrários. A otimização topológica tem sido comumente utilizada para minimizar a flexibilidade de estruturas sujeitas a restrições de volume. A ideia desta técnica é distribuir uma certa quantidade de material em uma estrutura, sujeita a carregamentos e condições de contorno, visando maximizar a sua rigidez. Neste trabalho, o objetivo é obter uma distribuição ótima de material de maneira a maximizar uma determinada frequência natural (para mantê-la afastada da frequência de excitação externa, por exemplo) ou maximizar a menor carga crítica linearizada (para garantir um nível mais elevado de estabilidade da estrutura). Malhas poligonais construídas usando diagramas de Voronoi são empregadas na solução do problema de otimização topológica. As variáveis de projeto, *i.e.* as densidades do material, utilizadas no processo de otimização, são associadas a cada elemento poligonal da malha. Vários exemplos de otimização topológica, tanto para problemas de frequências naturais de vibração quanto para cargas críticas linearizadas, são apresentados para demonstrar a funcionalidade e a aplicabilidade da metodologia proposta.

Palavras-chave

Otimização topológica; frequências naturais de vibração; carga crítica linearizada; problema de autovalor; elementos finitos poligonais.

Contents

List of Figures

List of Tables

Abbreviations

SIMP: Solid Isotropic Material with Penalization

RAMP: Rational Approximation of Material Properties

ESO: Evolutionary Structural Optimization

AM: Adjoint Method.

DDM: Direct Differentiation Method

FDM: Finite Difference Method

OC: Optimality Criteria

MMA: Method of Moving Asymptotes

FEM: Finite Element Method

dof: Degrees of freedom

Nomenclature

N_{el}**:** Number of elements in mesh

ε: Ersatz number

N_n**:** Number of nodes

$\boldsymbol{x}$**:** Vector of design variables

ρ_i**:** Density of element i

r_{min}: Filter radius

V**:** Volume

V_s**:** Upper bound on the final volume

$\boldsymbol{K}$**:** Global elastic stiffness matrix

$\boldsymbol{k}^e$**:** Element elastic stiffness matrix

$\boldsymbol{K}_\sigma$**:** Global geometric or stress stiffness matrix

$\boldsymbol{k}_\sigma^e$**:** Element geometric or stress stiffness matrix

$\boldsymbol{M}$**:** Global mass matrix

$\boldsymbol{m}^e$**:** Element mass matrix

$\boldsymbol{D}$**:** Constitutive matrix

$\boldsymbol{N}$**:** Shape function

$\boldsymbol{B}$**:** Strain-displacement matrix of shape function derivatives

$\boldsymbol{G}$**:** Stress matrix of shape function derivatives

$\boldsymbol{E}$**:** Young's modulus

$\boldsymbol{\nu}$**:** Poisson's ratio

$\boldsymbol{E}^0$**:** Young's modulus of solid material

p**:** Stiffness penalization parameter

g**:** Geometric or stress penalization parameter

q**:** Mass penalization parameter

$\boldsymbol{u}$**:** Global displacement vector

$\boldsymbol{f}$**:** Global force vector

λ_j**:** $j-th$ eigenvalue of structure

ω_j**:** $j-th$ eigenfrequency of structure

v_j**:** $j-th$ eigenvector of structure

$f(.)$**:** Objective function

$g(.)$**:** Constraint function

A_i**:** Area of the density element i in the initial domain

A_i^0**:** Area of the density element i in the reference domain

μ**:** Lagrange multiplier

"*La inteligencia es la capacidad de adaptarse al cambio.*"

Stephen Hawking

1.
Introduction

1.1
Motivation

Structural optimization problems can be classified into three types: sizing, shape, and topology optimization [1].

For sizing optimization, the shape of the structure is known, and the objective is to optimize the structure by adjusting the sizes of its components. Here, the design variables are the sizes of the structural elements, *e.g.*, the diameters of the bars or the thicknesses of a metal sheet. Figure 1.1(a) illustrates an example of size optimization where the diameter of the bars are the design variables.

For shape optimization, the design variables are the external contours of the domain and/or the shapes of internal pre-existing holes, as shown in Figure 1.1(b).

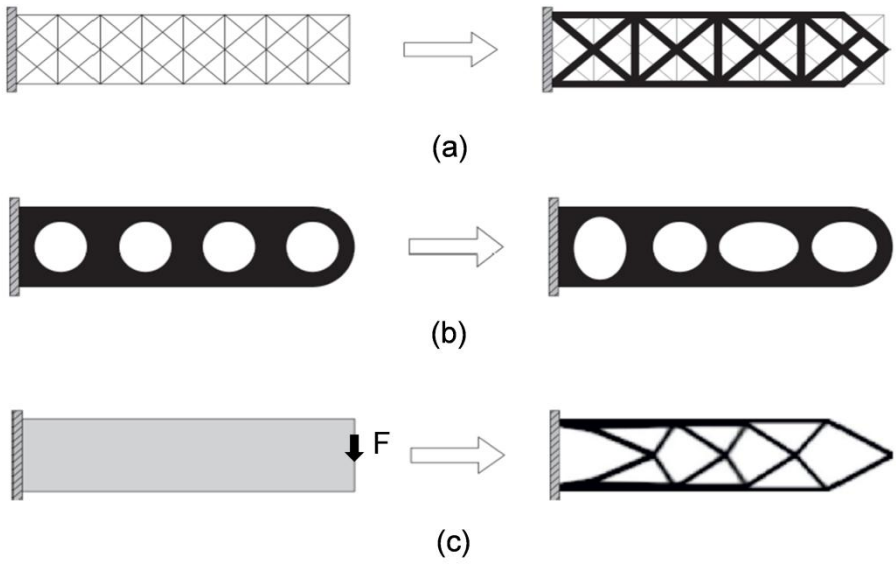

Figure 1.1: Different types of structural optimization. (a) Sizing optimization, (b) Shape optimization, and (c) Topology optimization. [2],[3].

Topology optimization is employed to find the optimum distribution of material in a given domain such that it minimizes specific performance measures, and is subjected to a volume constraint, as illustrated in Figure 1.1(c) [2]. In this work, we will focus on topology optimization.

In general, the structural optimization problem can be written as:

$$\begin{cases} \min \quad f(\boldsymbol{x}) & \boldsymbol{x} \in \Re^n \\ \text{s.t.} & \\ \quad h_k(\boldsymbol{x}) = 0\,, \; k = 1, \ldots, m \\ \quad c_l(\boldsymbol{x}) \leq 0\,, \quad l = 1, \ldots, p \\ \quad x_i^l \leq x_i \leq x_i^u\,, \; i = 1, \ldots, n \end{cases} \qquad (1\text{-}1)$$

where $f(\boldsymbol{x})$ is the objective function (*e.g.* compliance, given eigenvalue), $h_i(\boldsymbol{x})$ and $c_l(\boldsymbol{x})$ are the equality and inequality constraints of the problem (*e.g.* stress, fatigue, displacements), $\boldsymbol{x}$ is the vector of the design variables (*e.g.* density of each element), and x_i^l and x_i^u are the lower and upper bounds of the design variables, respectively.

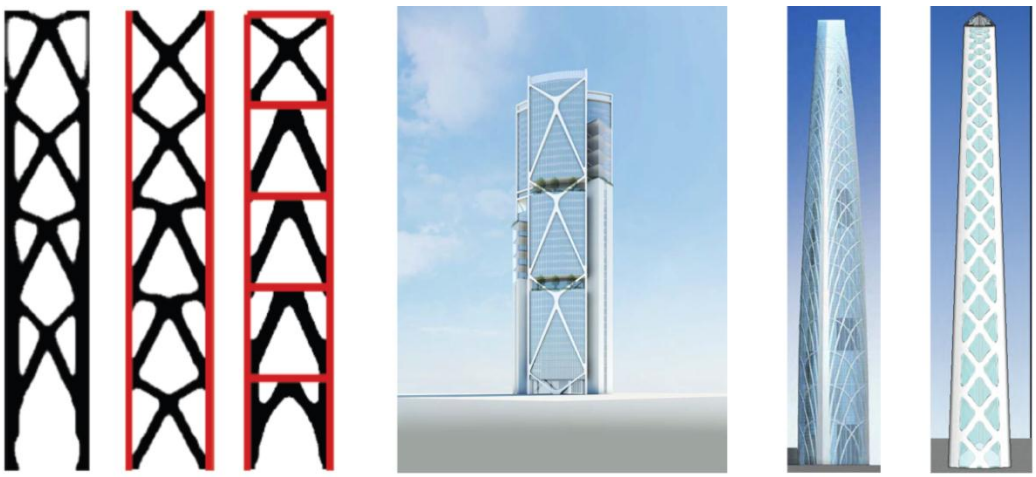

Figure 1.2: (a) Maximizing the overall stiffness of a building with volume constraints (b) Optimal building systems [4].

For a particular case of compliance minimization, the topology optimization problem can be expressed as:

$$\begin{cases} \min\limits_{\boldsymbol{x},\boldsymbol{u}} \quad f(\boldsymbol{x}) = \boldsymbol{f}^T\boldsymbol{u} \\ \text{s.t.} \\ \sum\limits_{i}^{N_{el}} V_i x_i - V_s \leq 0 \\ \boldsymbol{K}\boldsymbol{u} = \boldsymbol{f} \\ and \quad x_i \in [0\ 1], \quad i = 1, \dots, N_{el} \end{cases} \tag{1-2}$$

where $\boldsymbol{K}\boldsymbol{u} = \boldsymbol{f}$ is the set of equilibrium equations that arise from the finite element formulation for linear elasticity, which relates the stiffness matrix $\boldsymbol{K}$, nodal displacements $\boldsymbol{u}$, and the applied load vector $\boldsymbol{f}$. Here, the objective is to minimize the compliance of the structure (equivalent to maximize its stiffness), for a certain load and boundary conditions, subject to an upper bound V_s on the final volume of the structure, and $V_i x_i$ is the volume of each element. Figure 1.2 shows some examples of compliance minimization.

The checkerboard patterns problem has its origin in numerical approximation, when traditional low order finite elements (e.g. Q4) are used. Structured meshes using triangles and quads may lead to configurations that enable the formation of checkerboard and one-node connection problems.

We use unstructured polygonal finite element meshes to avoid checkerboard layouts and one-node connections [5].

Figure 1.3 shows an example, proposed by P. Browne [6], where checkerboard patterns appear when topology optimization is used for compliance minimization of a cantilever beam using conventional $Q4$ elements.

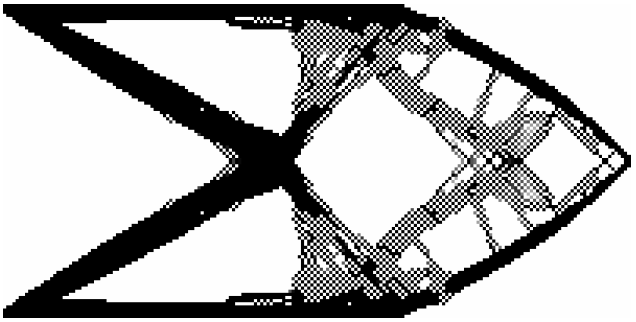

Figure 1.3: Checkerboard patterns in a cantilever beam problem using Q4 elements [6].

Figure 1.4 presents an example of topology optimization for compliance minimization using both standard regular quadrilateral elements and polygonal elements. Notice that the use of polygonal elements naturally eliminates the appearance of checkerboard patterns and one-node connections (see Reference [7] for more details.)

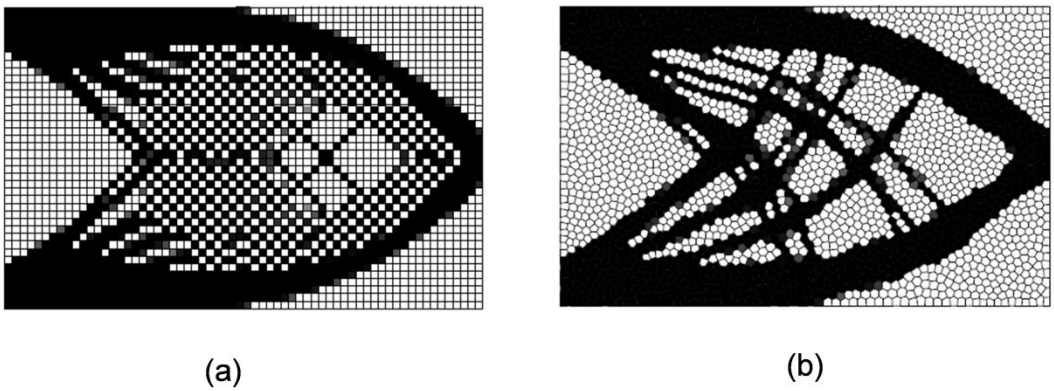

Figure 1.4: Topology Optimization for compliance minimization using: (a) 2560 Q4 elements and (b) 2560 polygonal elements ([7]).

Another advantange of polygonal elements is that they provide a great flexibility in discretizing complex domain, as shown in Figure 1.5.

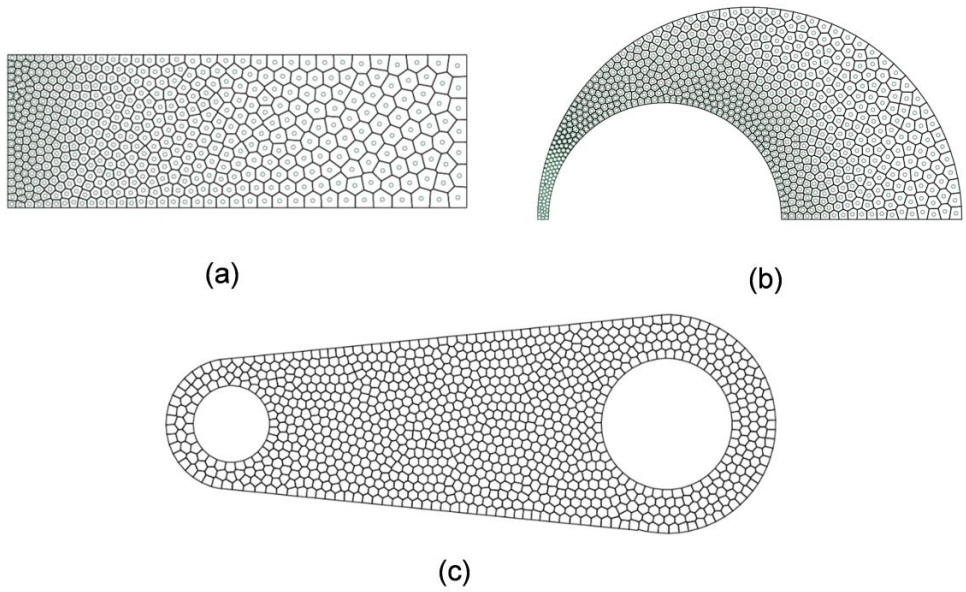

Figure 1.5: Polygonal meshes in different domains: (a) Rectangular; (b) Horn geometry and (c) Wrench geometry ([8])

The constrained geometry of the discretizations associated with standard triangles and quads can cause bias in the orientation of members, leading to mesh-dependent (sub-optimal) topology optimization designs [8]. Figure 1.6 shows that this problem can be easily cincumvented by using polygonal element meshes [8].

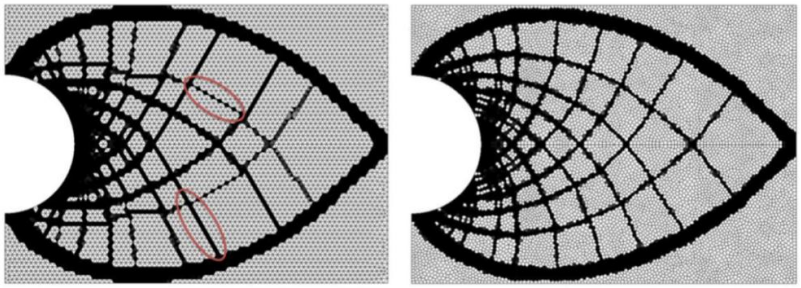

Figure 1.6: Topology optimization applied to the Michell Domain cantilever problem; (a) using $T6$ elements and (b) using Polygonal Elements ([8]).

When applied to fluid flow problems (*e.g.* Stokes flow), polygonal elements have shown to be naturally stable as illustrated in Figure 1.7 for a lid-driven cavity problem. As expected from the literature, the use of conventional Q4 elements leads to checkerboard layouts in the pressure field, (see Figure 1.7(a)). However, for polygonal elements, no checkerboard patterns are observed (see Figure 1.7 (b)).

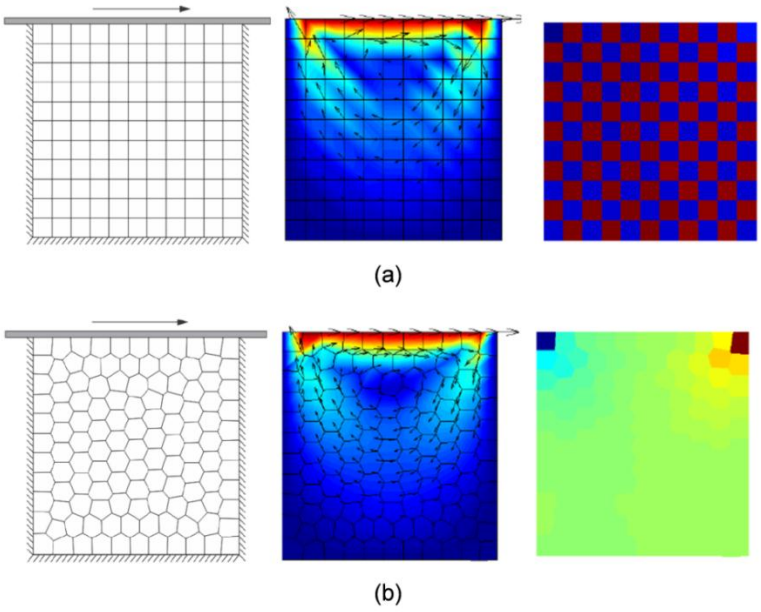

Figure 1.7: Velocity and pressure fields for a lid-driven cavity problem: (a) using $Q4$ elements and (b) using polygonal elements [9]).

Topology optimization can also be extended to other applications such as compliant mechanisms and dynamics. Figure 1.8 to 1.10 show some applications of topology optimization for structural problems (*e.g.* bridges, support tanks, aviation industry and wing design of airplanes).

Figure 1.8: Topology optimization applied to bridges [10] and support tanks [11].

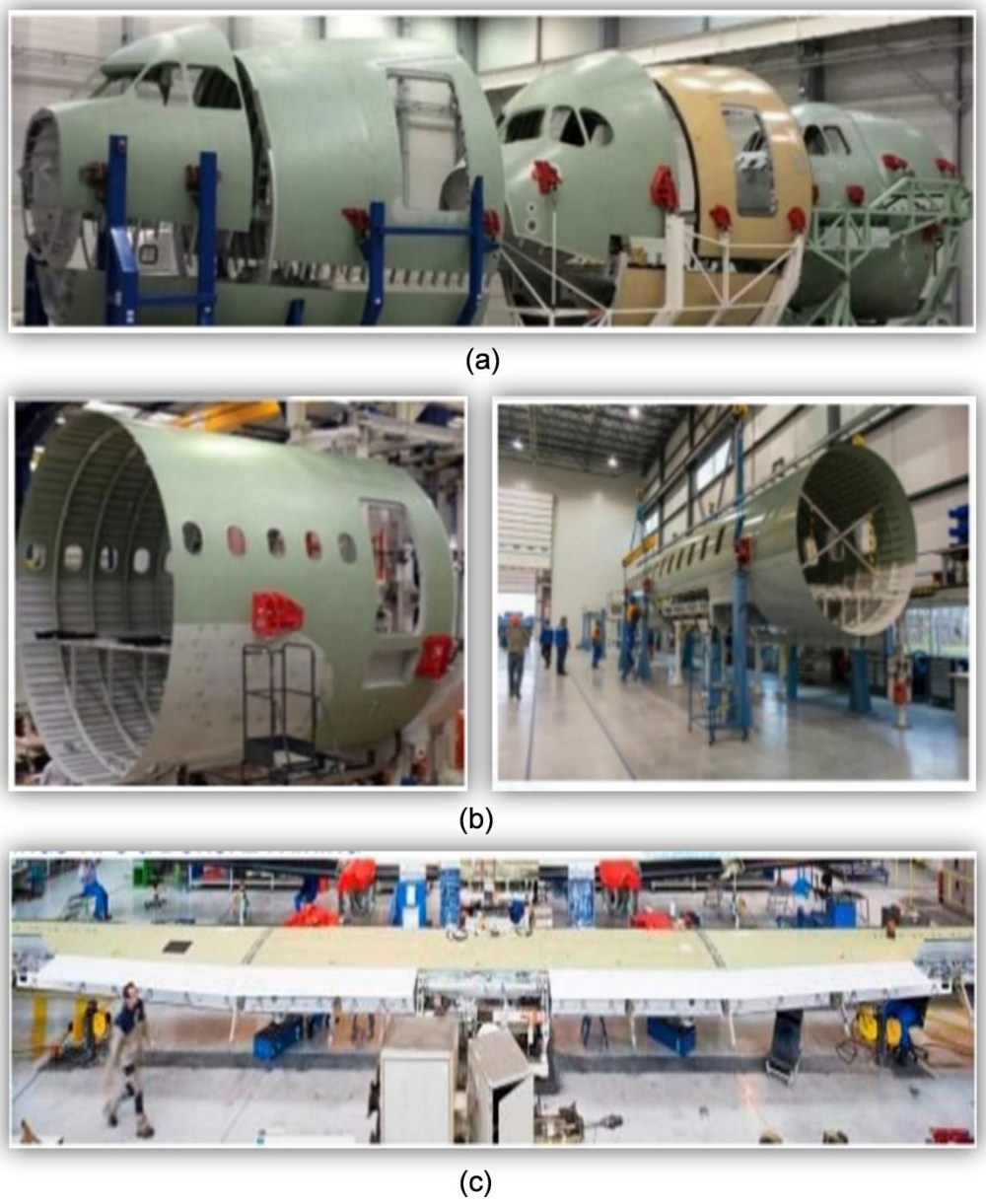

Figure 1.9: Aviation industry; (a) Airbus-Nose fuselage; (b) Airbus-Center fuselage and (c) wings tips [12].

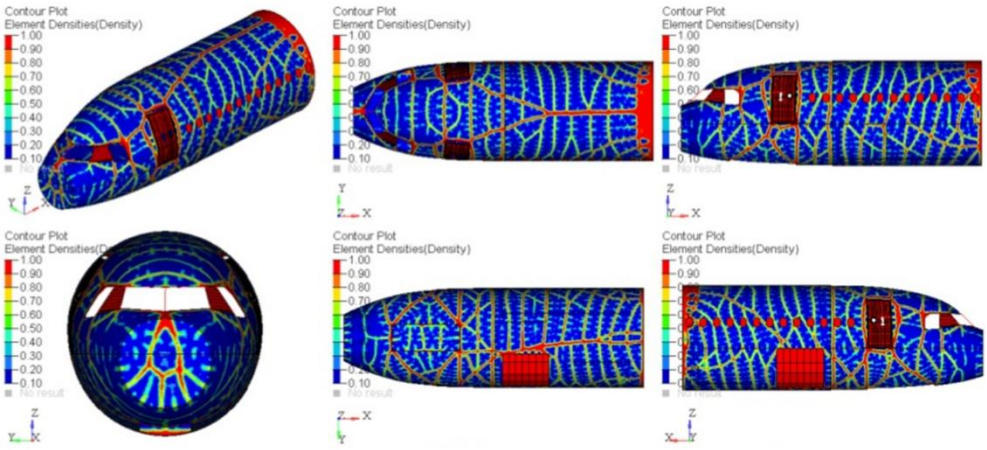

(a)

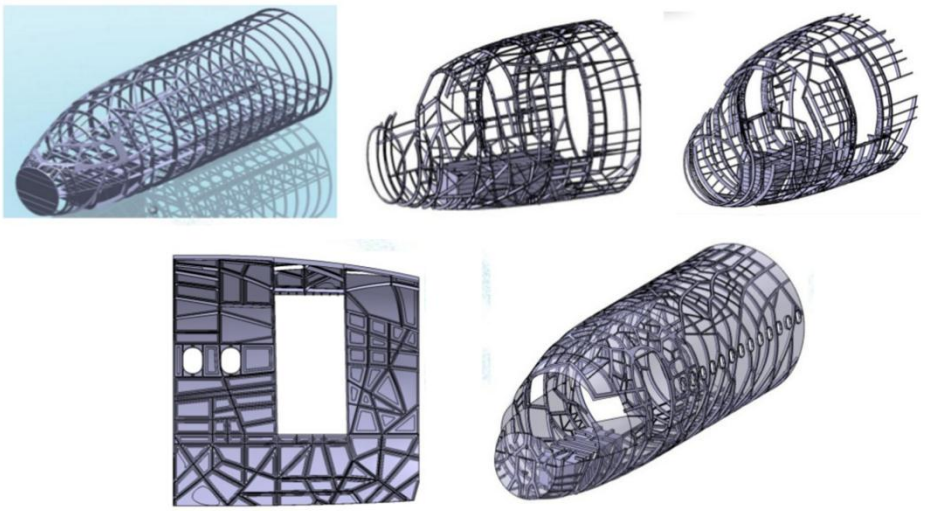

(b)

Figure 1.10: (a) Airbus/Nose and forward Fuselage and (b) Aircraft Architecture [12].

When topology optimization is applied to vibration problems, the idea is to design a structure with a reduced amount of material such that its range of natural frequencies can be shifted from the exciting external frequency value in order to avoid the resonance phenomenon.

Figure 1.11(a) illustrates a simply supported beam problem where the fundamental frequency $\omega_1 = 68\ Hz$ has been maximized to $\omega_1 = 205\ Hz$ and

Figure 1.11(b) illustrates a simply arc clamped beam where the initial difference between third and second eigenfrequencies $\omega_3 - \omega_2 = 119.7\ Hz$ has been maximized to $\omega_3 - \omega_2 = 319.2\ Hz$ [13].

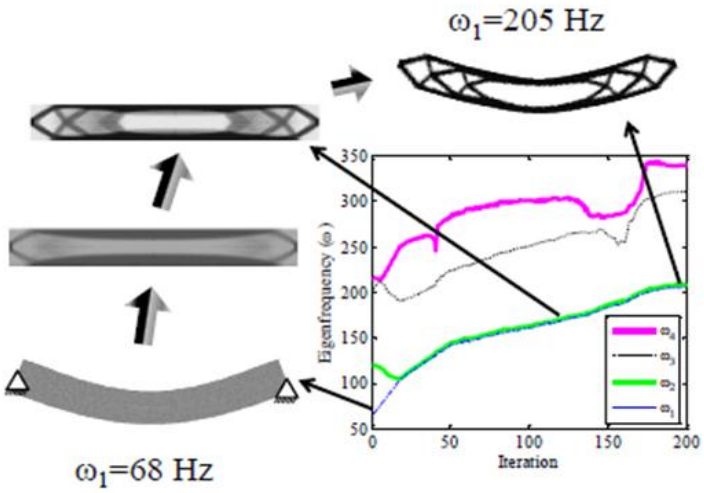

(a)

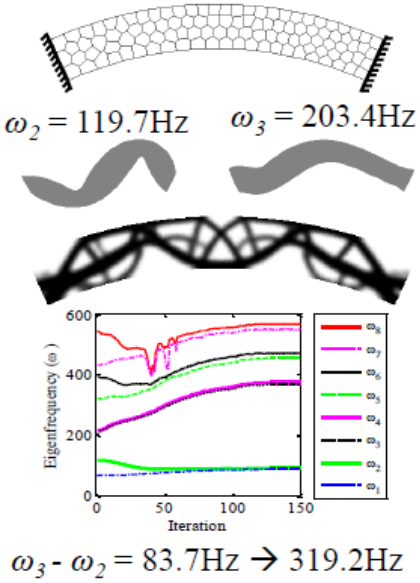

(b)

Figure 1.11: Examples of structural dynamic topology optimization [13].

On the contrary, when topology optimization is used for the design of slender structures under compression loads, the idea is to find an optimal material distribution in order to increase the lowest critical buckling load.

The general formulation of the topology optimization theory applied to a linearized buckling load problem can be written as:

$$
\begin{cases}
\max\limits_{x,u} \quad f(\boldsymbol{x}) = \lambda_{min} \\
\text{s.t.} \\
\sum\limits_{i} V_i x_i - V_s \leq 0 \\
\text{with} \\
\boldsymbol{K}\boldsymbol{u} = \boldsymbol{f} \\
\boldsymbol{K}\boldsymbol{v}_j + \lambda_j \boldsymbol{K}_{\boldsymbol{\sigma}}(\boldsymbol{x},\boldsymbol{u})\boldsymbol{v}_j = \boldsymbol{0}\,; \quad j = 1, \dots, N_{dof} \\
and \qquad x_i \in [0\ 1], \qquad i = 1, \dots, N_{elem}
\end{cases}
\tag{1-3}
$$

where $\boldsymbol{K}\boldsymbol{u} = \boldsymbol{f}$ is the set of finite element equilibrium equations for linear elasticity, and $(\boldsymbol{K} + \lambda_j \boldsymbol{K}_{\boldsymbol{\sigma}})v_j = \boldsymbol{0}$ is the eigenvalue problem to find the linearized critical load factor λ_{min}. Here, the objective is to maximize the lowest eigenvalue subject to an upper bound V_s on the final volume of the structure and $V_i x_i$ is the volume of each element [14].

Because the robustness and efficiency of the topology optimization scheme are obtained using gradient methods, it should be noted that the sensitivity analysis plays a very important role in the optimization process.

The level of complexity of sensitivity calculations depends on the type of objective function being considered in the topology optimization problem. To minimize the compliance and to solve eigenfrequency problems, it is easy to perform sensitivity calculations because the quantities involved are explicitly dependent on the design variable (*e.g.,* the material densities). However, for the linearized buckling problem, it is more difficult to derive the sensitivities because this objective function depends explicitly on the displacements, and also it depends implicitly on the material densities.

In this work, we provide a detailed derivation of the sensitivity equations that correspond to the three most well-known methods, which are available in the literature for topology optimization, and we compare their performances with respect to the computational efficiency.

1.2
Previous Work

The application of topology optimization to eigenvalue problems has recently been found in the literature. M. M. Neves et al. [15] investigated an approach to introduce critical load control into the topology optimization model. H. C. Rodrigues et al. [16] employed nonsmooth analysis tools to derive the required optimality conditions for maximizing the buckling load. Bendsøe and Sigmund [14] are the first reported paper to consider topology optimization for buckling problems by using Solid Isotropic Material with Penalization (SIMP). E. Lund [17] also reported the development of topology optimization for maximizing the buckling load factor of material composite shell structures by using Discrete Material Optimization (DMO).

P.A. Browne [6] applied the Evolutionary Structural Optimization (ESO) method to minimize the volume of the structure subject to compliance and buckling constraints. He employed the MMA as the optimizer method and used the fast binary descent algorithm. Spurious buckling modes have been discussed for compliance problem subjected to volume constraint. He presented different ways to overcome this problem.

S.J.Van den Boom [18] worked with topology optimization for structural compliance minimization considering both volume and buckling constraints. She developed the adjoint method using Q4 elements calculating the sensitivities of the objective and constraint functions, and also employed the MMA method as the optimizer. She discussed and showed some strategies to overcome problems such as negative buckling loads, mode switching, multiplicity of buckling loads and buckling of void elements (spurious buckling modes).

Quantian L. et al. [19] used a Moving Iso Surface Threshold method (MIST), where the lower bound of the eigenvalue was defined to eliminate spurious localized buckling modes.

Gao X. and Ma H. [20] applied topology optimization for structural compliance minimization considering constraints on both volume and buckling load factor.

Kim T. et al. [21] presented a parallel implementation of the topology optimization method for large-scale structural eigenvalue problems, where the sensitivity analysis and the update of the design variables were performed

independently in each subdomain with minimum data communications among the subdomains.

With respect to the application of topology optimization to dynamics, Bratus A. S. and Seiranian [22] investigated interesting applications in the optimal design of structures to maximize the lowest eigenfrequency by using a self-adjoint operator. Seiranian [23] also presented some applications of topology optimization for the multiple eigenvalue problem. Z. D. Ma et al. [24] used the concept of the mean-eigenvalue to maximize a specified eigenfrequency and the gap between eigenfrequencies by using Optimal Material Distribution [25]. Their approach was also applied to solve the stiffness maximization problem in forced vibration.

Xie Y. M. and Steven G. P. [26] and Huang X. et al. [27] applied the Evolutionary Structural Optimization (ESO) method to a wide range of frequency optimization problems, which include maximizing or minimizing a given frequency, the gap between two given frequencies, or multiple frequency constraint problems.

N. Olhoff and Du J. [28] and Du J and Olhoff N. [29] also applied topology optimization to the design of structures, where the eigenfrequencies are shifted from the external excitation frequency value to prevent the resonance problem. Yoon G. [30] investigated the same problem considering the geometrically nonlinear behavior of the structures.

N. Olhoff et al. [31] also investigated the optimum design of the band gap for beam structures.

Based on the recent developments reported by Talischi *et al.* [8] regarding the use of polygonal finite elements for topology optimization, F. Evgueni et al. [13] presented a multiresolution scheme for topology optimization, which was applied to dynamic problems.

1.3
Objective of this Dissertation

The main objective of this work is to present some applications of topology optimization for eigenvalue problems, such as natural frequency or linearized buckling load, using polygonal finite elements in arbitrary two-dimensional domains.

The specific objectives are:

1. To develop a numerical solution for computing the critical buckling load by using polygonal finite elements.
2. To derive the mathematical expressions for the sensitivities of the objective and constraint functions with respect to the design variables for both natural frequencies and linearized buckling problems by using the well-known sensitivity methods, namely, the Finite Difference Method (FDM), Direct Differentiation Method (DDM), and Adjoint Method (AM).
3. To solve the topology optimization problems for representative numerical examples, and to compare the obtained solutions with respect to the robustness and efficiency of the different sensitivity methods.

1.4
Outline of this Dissertation

The remainder of this work is organized as follows: In Chapter 2, we explain how to solve an eigenvalue problem by using the Finite Element Method (FEM) with polygonal meshes. In Chapter 3, we show how to compute the sensitivity of the eigenvalue with respect to design variables, which is one of the most important steps in the optimization process. In the case of the linearized buckling problem, we show different methods for computing the sensitivities, and compare the solutions with respect to the CPU time. In Chapter 4, we present the topology optimization applied to eigenfrequency and buckling problems, and define the objective and constraint functions and the optimization algorithm used here. Moreover, we discuss several numerical difficulties that arise when topology optimization is applied to the eigenvalue problem, such as multiplicity of eigenvalues and spurious mode. We also present some strategies to overcome these problems. In Chapter 5, we discuss the results obtained using several representative numerical examples. Finally, in Chapter 6, we summarize the conclusions of this work and present some suggestions for future work.

2.
Structural Eigenproblems

In this chapter, we discuss briefly the basic issues that are related to the computational steps for computing the natural frequencies and linearized buckling loads of a given structure. The domain is discretized based on the finite element method and we present the main matrices and equations associated with these problems.

2.1
Finite Element Discretization

The Finite Element Method (FEM) is a powerful numerical technique that is employed to solve differential equations that describe the physical behavior of structures. It consists of discretizing the domain into small elements (usually triangles or quadrilaterals), where for each element, the displacement field $\boldsymbol{u}$ is approximated by $\boldsymbol{u}^e$ as follows:

$$\boldsymbol{u}^e(\boldsymbol{x}) = \sum_{i=1}^{N_n} u_i \, N_i(\boldsymbol{x}) = \boldsymbol{N}\,\hat{\boldsymbol{u}} \qquad (2\text{-}1)$$

where N_i are the shape functions, $\hat{\boldsymbol{u}}$ are the nodal displacements of element e, and N_n is the total number of nodes in this element.

The strains can be obtained as:

$$\boldsymbol{\varepsilon} = \boldsymbol{\nabla}\boldsymbol{u}^e \qquad (2\text{-}2)$$

where $\boldsymbol{\nabla}$ is a linear operator.

From Equations (2-1) and (2-2), the strains can be related to the nodal displacements as:

$$\boldsymbol{\varepsilon} = \boldsymbol{\nabla}\,\boldsymbol{N}\,\hat{\boldsymbol{u}} \qquad (2\text{-}3)$$

The product $\boldsymbol{\nabla N}$ represents the strain-displacement matrix, also called $\boldsymbol{B}$, and for a specific 2D case, the above-mentioned vectors and matrices can be expressed as:

$$\boldsymbol{\varepsilon} = \begin{Bmatrix} \varepsilon_{xx} \\ \varepsilon_{yy} \\ \varepsilon_{xy} \end{Bmatrix}; \quad \boldsymbol{\nabla} = \begin{bmatrix} \partial/\partial x & 0 \\ 0 & \partial/\partial y \\ \partial/\partial y & \partial/\partial x \end{bmatrix}; \quad \boldsymbol{B}_i = \begin{bmatrix} \partial N_i/\partial x & 0 \\ \cdots \quad 0 & \partial N_i/\partial y \ \cdots \\ \partial N_i/\partial y & \partial N_i/\partial x \end{bmatrix} \qquad (2\text{-}4)$$

where $\boldsymbol{B}_i$ is a submatrix associated with node i of element e. For the plane stress case, which is the main focus of this work, the stresses can be written as:

$$\boldsymbol{\sigma} = \mathbf{D}\,\boldsymbol{\varepsilon}, \qquad (2\text{-}5)$$

where

$$\boldsymbol{D} = \frac{E}{1-\nu^2}\begin{bmatrix} 1 & \nu & 0 \\ \nu & 1 & 0 \\ 0 & 0 & \dfrac{1-\nu}{2} \end{bmatrix} \qquad (2\text{-}6)$$

is the material constitutive matrix, and E and ν are the Young modulus and Poisson ratio, respectively.

The element stiffness matrix can be computed using:

$$\boldsymbol{k} = \int_{V^e} \boldsymbol{B}^{\boldsymbol{T}} \boldsymbol{D}\, \boldsymbol{B}\, \mathrm{dV} \qquad (2\text{-}7)$$

where V^e denotes the element volume. The quantity $\boldsymbol{k}$ is evaluated by performing a numerical integration over volume V^e. The global stiffness matrix $\boldsymbol{K}$ can be obtained by assembling the elementary stiffness matrices. The final system of linear equations is given by $\boldsymbol{K}\boldsymbol{u} = \boldsymbol{f}$, where $\boldsymbol{f}$ is the global load vector and $\boldsymbol{u}$ is the unknown global displacement vector.

2.1.1 Polygonal Finite Elements

For polygonal elements, the finite element formulation that we adopted is based on the Laplace shape functions and isoparametric transformations (Talischi *et al.* [32]). The shape function evaluated at point $\boldsymbol{\xi}$ and corresponding to node i of a given reference n-gon, is defined as:

$$N_i(\boldsymbol{\xi}) = \frac{\alpha_i(\boldsymbol{\xi})}{\sum_{j=1}^{n} \alpha_j(\boldsymbol{\xi})} \qquad (2\text{-}8)$$

where

$$\alpha_i(\boldsymbol{\xi}) = \frac{A(\boldsymbol{p}_{i-1}, \boldsymbol{p}_i, \boldsymbol{p}_{i+1})}{A(\boldsymbol{p}_{i-1}, \boldsymbol{p}_i, \boldsymbol{\xi}) A(\boldsymbol{p}_i, \boldsymbol{p}_{i+1}, \boldsymbol{\xi})} \qquad (2\text{-}9)$$

and $A(\boldsymbol{a}, \boldsymbol{b}, \boldsymbol{c})$ is the area of the triangle defined by vertices $\boldsymbol{a}, \boldsymbol{b}, \boldsymbol{c}$, as illustrated in Figure 2.1.

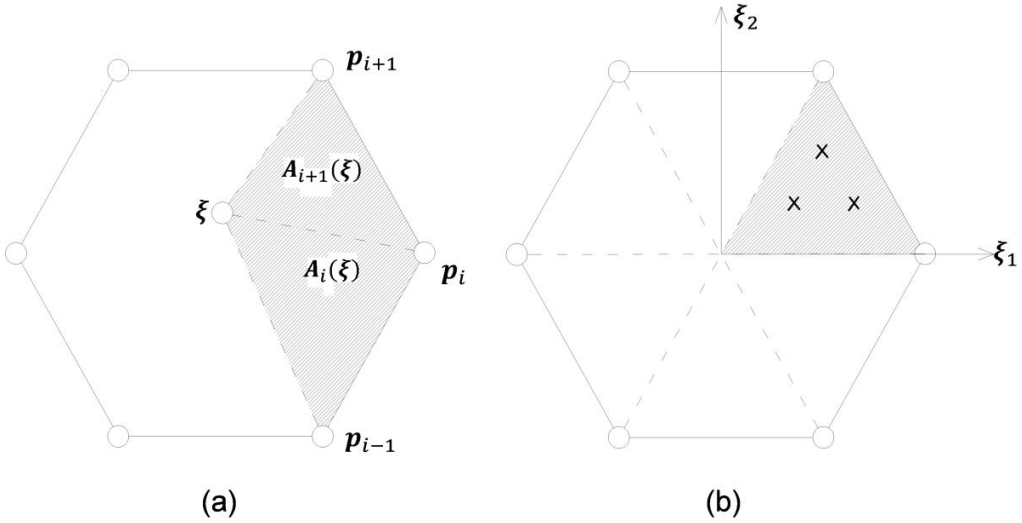

Figure 2.1: (a) Triangular areas used to compute shape functions of polygonal elements and (b) Triangulation of the reference regular polygonal and integration points defined on each triangle.

An isoparametric mapping from regular n-gons (the so-called “parent” element) to any convex polygon can be constructed using these shape functions. Because the interpolated field varies linearly on the boundary, the resulting approximation is conforming. Following the usual approach in the finite element community, the shape functions are defined on the parent domain, where the weak form integrals are evaluated numerically. The reference n-gon is divided into n triangles (by connecting the centroid to the vertices), and well-known quadrature rules are used on each triangle (see Talischi *et al.* [32] for more details).

2.2
Natural Frequencies

Neglecting damping effects, the natural frequencies of a given structure depend not only on the stiffness matrix, presented in Section 2.1, but also on the mass distribution along its domain.

The element mass matrix $\boldsymbol{m}$ is given by:

$$\boldsymbol{m} = \int_{V^e} \rho \ \boldsymbol{N^T N} \, \mathrm{dV} \qquad (2\text{-}10)$$

where ρ is the element density, $\boldsymbol{N}$ is a matrix containing the element shape functions defined in Equation (2-8) and V^e is the element domain (area).

The global mass matrix can be obtained by assembling each element mass matrix as:

$$\boldsymbol{M} = \sum_{e=1}^{N_{el}} \boldsymbol{m}^e \qquad (2\text{-}11)$$

where N_{el} is the total number of elements in the mesh.

The corresponding eigenproblem, which is associated with the natural frequencies of the structure, is given by:

$$(\boldsymbol{K} - \lambda \boldsymbol{M})\, \boldsymbol{v} = \boldsymbol{0} \qquad (2\text{-}12)$$

where λ represents the eigenvalues, *i.e.*, the square of the structural natural frequencies $\lambda = \omega^2$ and for each eigenvalue, $\boldsymbol{v}$ corresponds to a shape mode (for more details, see references R.Cook [33] and K.Bathe [34]).

2.3
Structural Linear Buckling Analysis

In this section, we present a general overview of the main steps that are required to solve the linearized buckling analysis problem.

First, we used the global stiffness matrix $\boldsymbol{K}$ and the applied load vector $\boldsymbol{f}$ to compute the global displacement vector $\boldsymbol{u}$, as:

$$\boldsymbol{K u} = \boldsymbol{f} \qquad (2\text{-}13)$$

Next, we obtain the element displacement vector $\boldsymbol{u}^e$ from global vector $\boldsymbol{u}$.

The element stresses $\boldsymbol{\sigma}$ can be determined using the element displacements $\boldsymbol{u}^e$, the material constitutive matrix $\boldsymbol{D}$, and the strain-displacement matrix $\boldsymbol{B}$ as:

$$\boldsymbol{\sigma} = \boldsymbol{DBu}^e \text{ ; where (for plane stress): } \boldsymbol{\sigma} = \{\sigma_x, \sigma_y, \tau_{xy}\}^T \quad (2\text{-}14)$$

Once the stresses are calculated, the element geometric (or stress) stiffness matrix can be obtained as:

$$\boldsymbol{k}_\sigma = \int_{V^e} \boldsymbol{G}^{\boldsymbol{T}} \boldsymbol{S}\, \boldsymbol{G}\, \mathrm{dV} \quad (2\text{-}15)$$

where $\boldsymbol{G}$ is an element matrix that contains shape functions and their derivatives, and $\boldsymbol{S}$ is a matrix that contains stress components, *i.e.*:

$$\boldsymbol{G}_i = \begin{bmatrix} \partial N_i/\partial x & 0 \\ \partial N_i/\partial y & 0 \\ \cdots & \cdots \\ 0 & \partial N_i/\partial x \\ 0 & \partial N_i/\partial y \end{bmatrix}; \qquad \boldsymbol{S} = \begin{bmatrix} \sigma_x & \tau_{xy} & 0 & 0 \\ \tau_{xy} & \sigma_y & 0 & 0 \\ 0 & 0 & \sigma_x & \tau_{xy} \\ 0 & 0 & \tau_{xy} & \sigma_y \end{bmatrix} \quad (2\text{-}16)$$

Now, for a discretized finite element mesh, the global geometric stiffness matrix can be calculated as:

$$\boldsymbol{K}_\sigma = \sum_{e=1}^{N_{el}} \boldsymbol{k}_\sigma^e \quad (2\text{-}17)$$

Finally, the eigenproblem corresponding to the linearized buckling problem can be established as:

$$(\boldsymbol{K} + \lambda \boldsymbol{K}_\sigma)\boldsymbol{v} = \boldsymbol{0} \quad (2\text{-}18)$$

where the eigenvalues λ correspond to the critical buckling loads, and for each eigenvalue, $\boldsymbol{v}$ corresponds to a shape buckling mode (see Bendsøe *et al.*, [14] for more details).

2.4
Numerical Examples

The first example consists of a 2D beam structure for which we compute the first four natural eigenfrequencies and the respective shape modes by using the expressions presented in the previous sections. The domain is discretized with polygonal finite elements. The geometry and boundary conditions are illustrated in Figure 2.2(a). The dimensions and material properties are: $E = 10^7$, $v = 0.3,\ h = 1,\ L = 30,\ \rho = 1$ and $t = 1$ (thickness). Table 2.1 shows the four eigenfrequencies that we obtained using different discretizations, together with the corresponding analytical solutions.

For the analytical solution we used reference by D.Inman [35] where the eigenfrequencies ω_n for the Euler-Beurnoulli beam theory are given by:

$$\omega_n = \beta_n^2 \sqrt{\frac{EI}{\rho A}} \quad , \qquad n = 1,2,3,\cdots \tag{2-19}$$

Considering the campled-clamped boundary condition, we arise at the following equation:

$$\cos(\beta L)\cosh(\beta L) = 0 \ , \qquad L \gg h \tag{2-20}$$

where, the solution is given by:

$$\beta_n L = \frac{(2n+1)\pi}{2}, n = 1,2,3\cdots \tag{2-21}$$

Table 2.1: First four eigenfrequencies for different discretizations.

	$\#of\ Elements$	$\#\ of\ Nodes$	$Eigenfrequencies\ \left(rad/s\right)$			
	N_{elem}	N_{nodes}	ω_1	ω_2	ω_3	ω_4
Numerical Solutions	1,000	1,895	22.72	62.03	120.11	195.52
	3,000	5,787	22.60	61.70	119.47	194.45
	5,000	9,687	22.57	61.64	119.33	194.23
	10,000	19,539	22.55	61.59	119.23	194.06
	20,000	39,283	22.54	61.56	119.18	193.98
Analytical Solutions			**22.52**	**62.56**	**122.63**	**202.71**

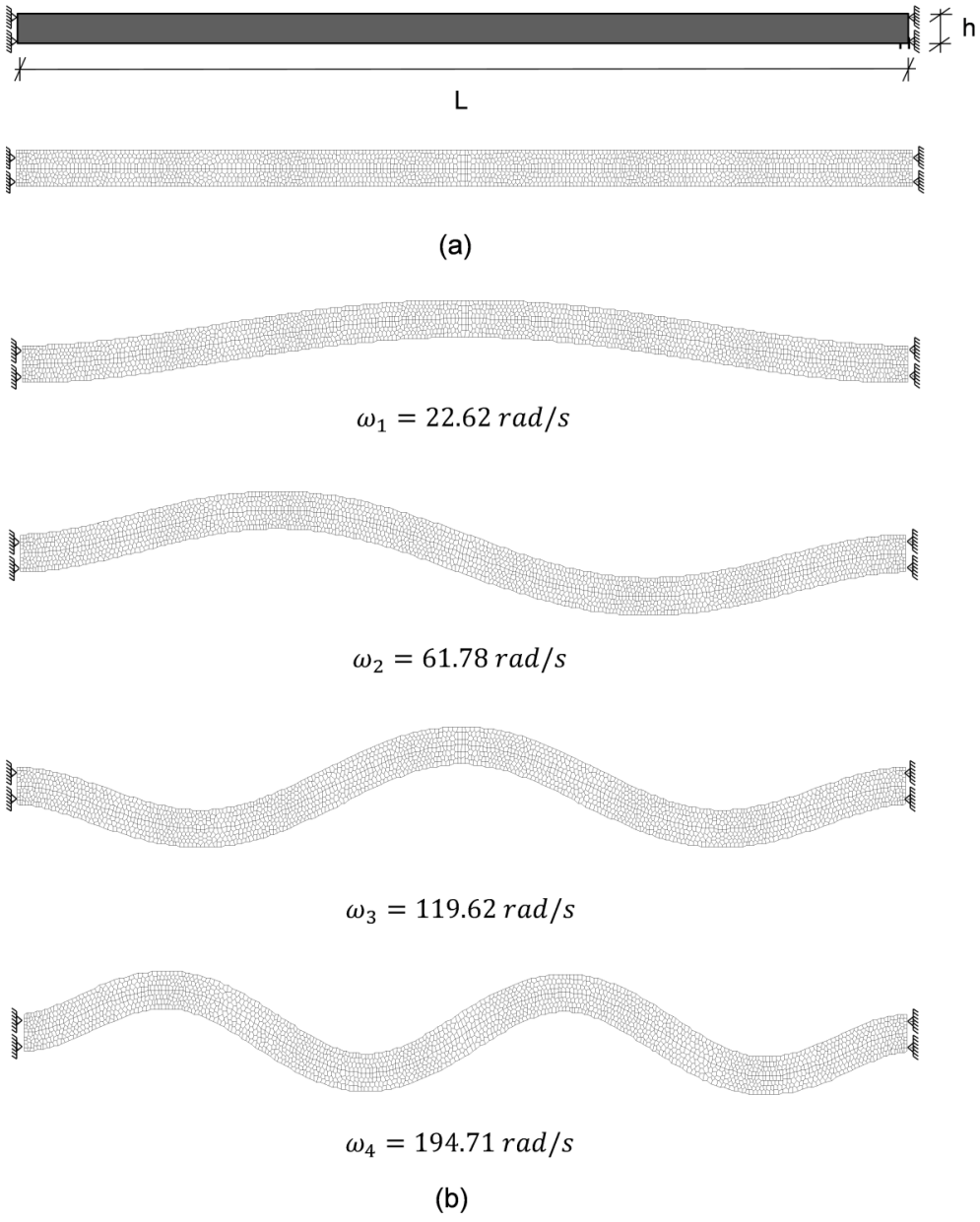

Figure 2.2: (a) Geometry and boundary conditions – (using 2,000 polygonal finite elements mesh) and (b) first four mode shapes.

The second example consists of a slender column subjected to a compressive distributed load f. The geometry, loads and boundary conditions are illustrated in Figure 2.3(a). The dimensions and material properties are: $E = 10^6, v = 0.3,\ h = 1,\ p = 1,\ L = 30,$ and $t = 1$ (thickness). Table 2.2 shows our numerical solutions of the first linearized buckling loads using different discretizations with polygonal meshes ($P_{crit_{numeric}}$) and the corresponding analytical solution ($P_{crit_{analytic}}$) using the Euler-Bernoulli column theory.

The expression for the critical buckling load of columns using Euler-Beurnoulli theory is given by [36],[37]:

$$P_{crit_{analytic}} = \frac{n^2\pi^2 EI}{4L^2} \quad , \qquad n = 1,2,3,\ldots \tag{2-22}$$

where, for slender columns, we should consider:

$$L \gg h \tag{2-23}$$

Table 2.2: Linearized critical buckling load.

$\#\ of\ Elements$	$\#\ of\ Nodes$	$Linearized\ critical\ load$
N_{elem}	N_{node}	$P_{crit_{numeric}}$
500	999	236.5615
1,000	1,993	231.8729
2,000	3,990	230.1616
4,000	7,961	229.2469
8,000	15,935	228.8001
12,000	23,915	228.6463
20,000	39,820	228.5254
40,000	79,661	228.4307
$P_{crit_{analytic}}$		**228.4630**

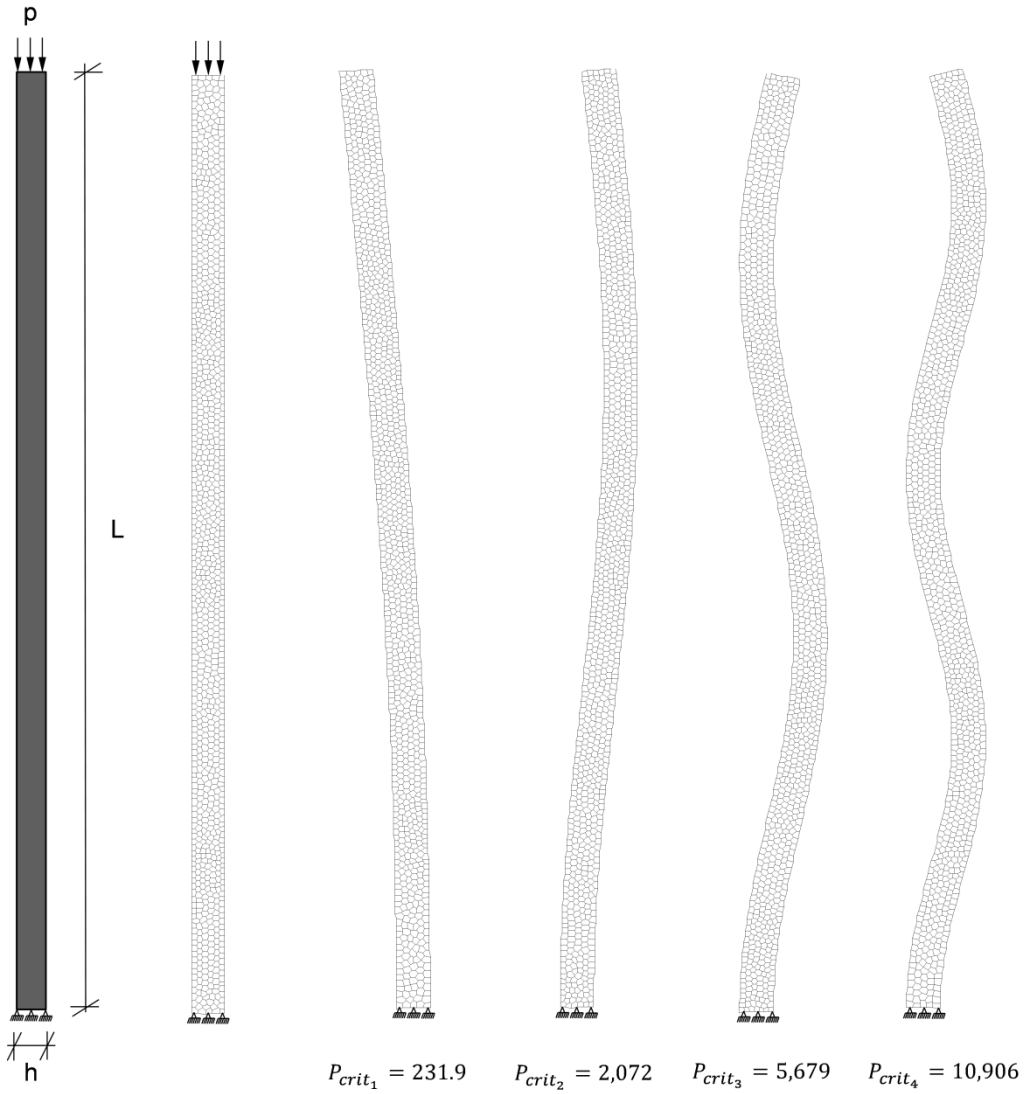

Figure 2.3: (a) Geometry, loading and boundary conditions – (using 1,000 polygonal finite elements mesh); and (b) first four buckling modes.

3.
Structural Sensitivity Analysis

In this chapter, we derive the sensitivities of the natural frequency of the vibration and buckling load with respect to the design variables. As shown in Sections 2.2 and 2.3 of Chapter 2, these response measures are eigenvalues of a generalized eigenvalue problem.

3.1
Eigenvalue Sensitivity Analysis

Consider the formulation for the natural frequency or buckling ($\boldsymbol{M} = -\boldsymbol{K}_\sigma$ for buckling problems) described by the following eigenvalue problem:

$$(\boldsymbol{K} - \lambda \boldsymbol{M})\boldsymbol{v} = \boldsymbol{0} \qquad (3\text{-}1)$$

Differentiating with respect to the design variable x, we have:

$$\left(\frac{\partial \boldsymbol{K}}{\partial x} - \frac{\partial \lambda}{\partial x}\boldsymbol{M} - \lambda\frac{\partial \boldsymbol{M}}{\partial x}\right)\boldsymbol{v} + (\boldsymbol{K} - \lambda \boldsymbol{M})\frac{\partial \boldsymbol{v}}{\partial x} = \boldsymbol{0} \qquad (3\text{-}2)$$

By multiplying the left side by $\boldsymbol{v}^T$, we obtain:

$$\boldsymbol{v}^T\left(\frac{\partial \boldsymbol{K}}{\partial x} - \frac{\partial \lambda}{\partial x}\boldsymbol{M} - \lambda\frac{\partial \boldsymbol{M}}{\partial x}\right)\boldsymbol{v} + \boldsymbol{v}^T(\boldsymbol{K} - \lambda \boldsymbol{M})\frac{\partial \boldsymbol{v}}{\partial x} = 0 \qquad (3\text{-}3)$$

Considering that the term $\boldsymbol{v}^T(\boldsymbol{K} - \lambda \boldsymbol{M})$ must vanish from Equation (3-1) and rearranging, we obtain:

$$\frac{\partial \lambda}{\partial x} = \frac{\boldsymbol{v}^T\left(\frac{\partial \boldsymbol{K}}{\partial x} - \lambda\frac{\partial \boldsymbol{M}}{\partial x}\right)\boldsymbol{v}}{\boldsymbol{v}^T\boldsymbol{M}\boldsymbol{v}} \qquad (3\text{-}4)$$

Note that for the buckling load, the global geometric stiffness matrix also depends on $\boldsymbol{u}$, which is implicitly dependent on the design x. The sensitivity of $\boldsymbol{K}_\sigma$ can thus be expressed as:

$$\frac{\partial \boldsymbol{K}_\sigma}{\partial x} = \left.\frac{\partial \boldsymbol{K}_\sigma}{\partial x}\right|_{\boldsymbol{u}=const} + \frac{\partial \boldsymbol{K}_\sigma}{\partial \boldsymbol{u}}\frac{\partial \boldsymbol{u}}{\partial x} \qquad (3\text{-}5)$$

Replacing $\boldsymbol{M} = -\boldsymbol{K}_\sigma$ in Equation (3-4) and using Equation (3-5), we have

$$\frac{\partial \lambda}{\partial x} = -\frac{\boldsymbol{v}^T \left[\frac{\partial \boldsymbol{K}}{\partial x} + \lambda \left(\frac{\partial \boldsymbol{K}_\sigma}{\partial x}\Big|_{\boldsymbol{u}=const} + \frac{\partial \boldsymbol{K}_\sigma}{\partial \boldsymbol{u}} \frac{\partial \boldsymbol{u}}{\partial x}\right)\right] \boldsymbol{v}}{\boldsymbol{v}^T \boldsymbol{K}_\sigma \boldsymbol{v}} \quad (3\text{-}6)$$

By rearranging Equation (3-6), we get:

$$\frac{\partial \lambda}{\partial x} = -\frac{\boldsymbol{v}^T \left[\frac{\partial \boldsymbol{K}}{\partial x} + \lambda \left(\frac{\partial \boldsymbol{K}_\sigma}{\partial x}\Big|_{\boldsymbol{u}=const}\right)\right] \boldsymbol{v} + \lambda \boldsymbol{v}^T \frac{\partial \boldsymbol{K}_\sigma}{\partial \boldsymbol{u}} \frac{\partial \boldsymbol{u}}{\partial x} \boldsymbol{v}}{\boldsymbol{v}^T \boldsymbol{K}_\sigma \boldsymbol{v}} \quad (3\text{-}7)$$

Using

$$\frac{\partial \boldsymbol{K}_\sigma}{\partial \boldsymbol{u}} \frac{\partial \boldsymbol{u}}{\partial x} = \sum_{j=1}^{l} \frac{\partial \boldsymbol{K}_\sigma}{\partial u_j} \frac{\partial u_j}{\partial x}, \quad (3\text{-}8)$$

where l is the number of degrees of freedom (DOF) of the structure, and

$$q_j = \boldsymbol{v}^T \frac{\partial \boldsymbol{K}_\sigma}{\partial u_j} \boldsymbol{v},$$

we can write

$$\frac{\partial \lambda}{\partial x} = -\frac{\boldsymbol{v}^T \left(\frac{\partial \boldsymbol{K}}{\partial x} + \lambda \frac{\partial \boldsymbol{K}_\sigma}{\partial x}\Big|_{\boldsymbol{u}=const}\right) \boldsymbol{v} + \lambda \boldsymbol{q}^T \frac{\partial \boldsymbol{u}}{\partial x}}{v^T \boldsymbol{K}_\sigma v} \quad (3\text{-}9)$$

Note that, for the case of the natural frequencies, we have $\boldsymbol{q} = \boldsymbol{0}$ and $\boldsymbol{K}_\sigma = -\boldsymbol{M}$ and the Equation (3-4) is restored.

The evaluation of Equation (3-9) can be done using either the Direct Differentiation Method (DDM) or the Adjoint Method (AM). The former directly solves $\frac{\partial \boldsymbol{u}}{\partial x}$ and then computes Equation (3-9). In order to avoid the computation of $\frac{\partial \boldsymbol{u}}{\partial x}$, the latter method constructs an adjoint problem that solves for the adjoint variable. These methods will be discussed in subsequent sections.

3.1.1
Direct Differentiation Method (DDM)

From the static equilibrium problem, $\boldsymbol{Ku} = \boldsymbol{f}$, we derive both members with respect to the design variable:

$$\frac{\partial \boldsymbol{f}}{\partial x} = \frac{\partial \boldsymbol{K}}{\partial x}\boldsymbol{u} + \boldsymbol{K}\frac{\partial \boldsymbol{u}}{\partial x} \quad (3\text{-}10)$$

Considering that the force vector $\boldsymbol{f}$ does not depend on the design variable x, $\frac{\partial \boldsymbol{f}}{\partial x}$ must be zero. By replacing it in Equation (3-10) and isolating the term $\frac{\partial \boldsymbol{u}}{\partial x}$, we have:

$$\frac{\partial \boldsymbol{u}}{\partial x} = -\boldsymbol{K}^{-1}\frac{\partial \boldsymbol{K}}{\partial x}\boldsymbol{u} \quad (3\text{-}11)$$

These solutions were obtained in an efficient manner because the stiffness matrix $\boldsymbol{K}$ was previously factored during the structural analysis step. Using $\frac{\partial \boldsymbol{u}}{\partial x}$ from Equation (3-11), $\frac{\partial \lambda}{\partial x}$ may now be directly calculated from Equation (3-9). However, in topology optimization, numerous design variables are required, making this approach impractical. As shown in the next section, we can obtain a very simple and efficient sensitivity expression by using the adjoint method.

3.1.2
Adjoint Method (AM)

Using Equation (3-11) in Equation (3-9), we obtain:

$$\frac{\partial \lambda}{\partial x} = -\frac{\boldsymbol{v}^T\left(\frac{\partial \boldsymbol{K}}{\partial x} + \lambda\frac{\partial \boldsymbol{K}_\sigma}{\partial x}\Big|_{\boldsymbol{u}=const}\right)\boldsymbol{v} - \lambda\boldsymbol{q}^{\boldsymbol{T}}\boldsymbol{K}^{-1}\frac{\partial \boldsymbol{K}}{\partial x}\boldsymbol{u}}{\boldsymbol{v}^T\boldsymbol{K}_\sigma\boldsymbol{v}} \quad (3\text{-}12)$$

The main idea here is to directly compute the term $\boldsymbol{q}^{\boldsymbol{T}}\boldsymbol{K}^{-1}$ by defining it as the adjoint variable $\boldsymbol{w}$:

$$\boldsymbol{Kw} = \boldsymbol{q} \quad (3\text{-}13)$$

Finally, by substituting Equation (3-13) in Equation (3-12), we obtain the general formulation for the eigenvalue-buckling sensitivity as:

$$\frac{\partial \lambda}{\partial x} = -\frac{\boldsymbol{v}^T \left(\frac{\partial \boldsymbol{K}}{\partial x} + \lambda \frac{\partial \boldsymbol{K}_\sigma}{\partial x}\Big|_{\boldsymbol{u}=const} \right) \boldsymbol{v} - \lambda \boldsymbol{w}^T \frac{\partial \boldsymbol{K}}{\partial x} \boldsymbol{u}}{\boldsymbol{v}^T \boldsymbol{K}_\sigma \boldsymbol{v}} \quad (3\text{-}14)$$

Note that the computation of $\boldsymbol{w}$ in Equation (3-13) is independent of the design variable x, which makes this approach very attractive for topology optimization.

3.2 Derivative of Elastic Stiffness and Mass Matrices

The explicit expression of the elastic stiffness matrix $\boldsymbol{K}$ is presented in Equation (2-7). Assuming a linear dependence of $\boldsymbol{D}_e$ on x_e, as expressed by $\boldsymbol{D}_e = x_e \boldsymbol{D}_e^0$, we can write the stiffness matrix as follows:

$$\boldsymbol{K} = \sum_{e=1}^{\boldsymbol{N_{el}}} \int_{\boldsymbol{\Omega_e}} x_e \boldsymbol{B}_e^T \boldsymbol{D}_e^0 \boldsymbol{B}_e d\Omega \quad (3\text{-}15)$$

where $\boldsymbol{D}_e^0$ is the constitutive matrix of the solid material. The derivative of $\boldsymbol{K}$ with respect to the design variable x_i is carried out on the element level as follows:

$$\frac{\partial \boldsymbol{K}}{\partial x_i} = \sum_{e=1}^{\boldsymbol{N_{el}}} \int_{\Omega_e} x_e \boldsymbol{B}_e^T \boldsymbol{D}_e^0 \boldsymbol{B}_e d\Omega = \sum_{e=1}^{\boldsymbol{N_{el}}} \int_{\Omega_e} \delta_{ie} \boldsymbol{B}_e^T \boldsymbol{D}_e^0 \boldsymbol{B}_e d\Omega \quad (3\text{-}16)$$

and

$$\frac{\partial \boldsymbol{K}}{\partial x_e} = \int_{\boldsymbol{\Omega_e}} \boldsymbol{B}_e^T \boldsymbol{D}_e^0 \boldsymbol{B}_e d\Omega = \boldsymbol{k}_e^0 \quad (3\text{-}17)$$

where $\boldsymbol{k}_e^0$ is the local stiffness matrix of the solid phase.

Similarly, to determine the elastic stiffness matrix, the derivative of the mass matrix can be given by:

$$\frac{\partial \boldsymbol{M}}{\partial x_e} = \int_{\boldsymbol{\Omega_e}} \rho_e^0 \boldsymbol{N}_e^T \boldsymbol{N}_e d\Omega = \boldsymbol{m}_e^0 \quad (3\text{-}18)$$

where ρ^0 and $\boldsymbol{m}_e^0$ are the density and local mass matrix of the solid phase, respectively.

3.3
Derivative of Geometric Stiffness Matrix

The geometric stiffness matrix is implicitly dependent on the design variable x through the displacement vector $\boldsymbol{u}$. From Equation (3-5) and Equation (3-8) the sensitivity of $\boldsymbol{K}_\sigma$ can thus be expressed as:

$$\frac{\partial \boldsymbol{K}_\sigma}{\partial x} = \frac{\partial \boldsymbol{K}_\sigma}{\partial x}\bigg|_{\boldsymbol{u}=const} + \sum_{j=1}^{l} \frac{\partial \boldsymbol{K}_\sigma}{\partial u_j}\frac{\partial u_j}{\partial x} \qquad (3\text{-}19)$$

The first term of Equation (3-19) represents the explicit dependence on the design, while the second term shows the implicit dependence through the displacement $\boldsymbol{u}(x)$. The explicit part is obtained as:

$$\frac{\partial \boldsymbol{K}_\sigma}{\partial x_i}\bigg|_{\boldsymbol{u}=const} = \sum_{e=1}^{N_{el}} \int_\Omega \boldsymbol{G}_e^T \frac{\partial \boldsymbol{S}_e}{\partial x_i}\bigg|_{\boldsymbol{u}=const} \boldsymbol{G}_e d\Omega_e \qquad (3\text{-}20)$$

From Equation (2-16), $\boldsymbol{S}_e$ is the elemental stress matrix. For the case of plane stress, we have:

$$\boldsymbol{S}_e = \begin{bmatrix} \sigma_x & \tau_{xy} & 0 & 0 \\ \tau_{xy} & \sigma_y & 0 & 0 \\ 0 & 0 & \sigma_x & \tau_{xy} \\ 0 & 0 & \tau_{xy} & \sigma_y \end{bmatrix} \qquad (3\text{-}21)$$

Deriving the stress matrix $\boldsymbol{S}_e$ with respect to the design variable x_i, and by considering the displacement $\boldsymbol{u}$ constant, we obtain:

$$\frac{\partial \boldsymbol{S}_e}{\partial x_i}\bigg|_{u=const} = \begin{bmatrix} \frac{\partial \sigma_x}{\partial x_i}\Big|_{u=const} & \frac{\partial \tau_{xy}}{\partial x_i}\Big|_{u=const} & & \\ \frac{\partial \tau_{xy}}{\partial x_i}\Big|_{u=const} & \frac{\partial \sigma_y}{\partial x_i}\Big|_{u=const} & & \\ & & \frac{\partial \sigma_x}{\partial x_i}\Big|_{u=const} & \frac{\partial \tau_{xy}}{\partial x_i}\Big|_{u=const} \\ & & \frac{\partial \tau_{xy}}{\partial x_i}\Big|_{u=const} & \frac{\partial \sigma_y}{\partial x_i}\Big|_{u=const} \end{bmatrix} \qquad (3\text{-}22)$$

The elemental stress components can be computed as:

$$\boldsymbol{\sigma}_e = \begin{Bmatrix} \sigma_x \\ \sigma_y \\ \tau_{xy} \end{Bmatrix} = x_e \boldsymbol{D}_e^0 \boldsymbol{B}_e \boldsymbol{u}_e \tag{3-23}$$

Deriving Equation (3-23) with respect to x_i:

$$\left.\frac{\partial \boldsymbol{\sigma}_e}{\partial x_i}\right|_{u=const} = \begin{Bmatrix} \left.\frac{\partial \sigma_x}{\partial x_i}\right|_{u=const} \\ \left.\frac{\partial \sigma_y}{\partial x_i}\right|_{u=const} \\ \left.\frac{\partial \tau_{xy}}{\partial x_i}\right|_{u=const} \end{Bmatrix} = \delta_{ie} \boldsymbol{D}_e^0 \boldsymbol{B}_e \boldsymbol{u}_e \tag{3-24}$$

and

$$\left.\frac{\partial \boldsymbol{\sigma}_e}{\partial x_e}\right|_{u=const} = \boldsymbol{D}_e^0 \boldsymbol{B}_e \boldsymbol{u}_e = \boldsymbol{\sigma}_e^0 \tag{3-25}$$

Finally, we obtain the explicit part of the derivative of the geometric stiffness as:

$$\left.\frac{\partial \boldsymbol{K}_\sigma}{\partial x_e}\right|_{\boldsymbol{u}=const} = \int_\Omega \boldsymbol{G}_e^T \boldsymbol{S}_e|_{\boldsymbol{\sigma}_e = \boldsymbol{\sigma}_e^0} \boldsymbol{G}_e d\Omega_e \tag{3-26}$$

Now, for the implicit part, we have:

$$\frac{\partial \boldsymbol{K}_\sigma}{\partial u_j} = \sum_{e=1}^{N_{el}} \int_\Omega \boldsymbol{G}_e^T \frac{\partial \boldsymbol{S}_e}{\partial u_j} \boldsymbol{G}_e d\Omega_e \tag{3-27}$$

Deriving the stress matrix $\boldsymbol{S}_e$, we obtain:

$$\frac{\partial \boldsymbol{S}_e}{\partial u_j} = \begin{bmatrix} \frac{\partial \sigma_x}{\partial u_j} & \frac{\partial \tau_{xy}}{\partial u_j} & & \\ \frac{\partial \tau_{xy}}{\partial u_j} & \frac{\partial \sigma_y}{\partial u_j} & & \\ & & \frac{\partial \sigma_x}{\partial u_j} & \frac{\partial \tau_{xy}}{\partial u_j} \\ & & \frac{\partial \tau_{xy}}{\partial u_j} & \frac{\partial \sigma_y}{\partial u_j} \end{bmatrix} \tag{3-28}$$

The derivative of the elemental stress components can be computed as:

$$\frac{\partial \boldsymbol{\sigma}_e}{\partial u_j} = \begin{Bmatrix} \dfrac{\partial \sigma_x}{\partial u_j} \\ \dfrac{\partial \sigma_y}{\partial u_j} \\ \dfrac{\partial \tau_{xy}}{\partial u_j} \end{Bmatrix} = x_e \boldsymbol{D}_e^0 \boldsymbol{B}_e \frac{\partial \boldsymbol{u}_e}{\partial u_j} \qquad (3\text{-}29)$$

Note that the term $\frac{\partial \boldsymbol{u}_e}{\partial u_j}$ is computed for each DOF of the structure. For the jth DOF, we have:

$$\frac{\partial \boldsymbol{u}_e}{\partial u_j} = \begin{Bmatrix} 0 \\ \vdots \\ 1 \\ \vdots \\ 0 \end{Bmatrix} \rightarrow u_j \qquad (3\text{-}30)$$

The calculation of the derivatives of the geometric stiffness matrix is the main computational cost associated with buckling topology optimization. For each variable $x_i = 1, \dots, n_{vp}$, we must compute Equation (3-14). This equation requires Equations (3-8) and (3-29), which contain a sum over $e = 1, \dots, N_{el}$ and $j = 1, \dots, N_{DOF}$, significantly increasing the computational cost. To reduce the computational cost, we computed and stored the node-element adjacency list to avoid any looping through the elements that do not have the DOF j.

3.4 Finite Difference Method (FDM)

A simple technique that is employed to compute the sensitivity with respect to the design variable is an approximation of the finite difference method. This technique is computationally expensive, but easy to implement, and is therefore used primarily for comparison with other methods.

A simple approximation for the derivative of a function $F(\boldsymbol{x})$, $\frac{\partial F}{\partial x_j}$, is the first order finite difference $\frac{\Delta F}{\Delta x_j}$, given by:

$$\frac{\Delta F}{\Delta x_j} = \frac{F\left(\boldsymbol{x} + \Delta x \boldsymbol{e}_j\right) - F(\boldsymbol{x})}{\Delta x} \qquad (3\text{-}31)$$

where:

$$\boldsymbol{e}_j = \begin{Bmatrix} 0 \\ \vdots \\ 1 \\ \vdots \\ 0 \end{Bmatrix} \rightarrow j \qquad (3\text{-}32)$$

Here, Δx is a small numerical perturbation, generally defined by:

$$\Delta x = \eta x_j \qquad (3\text{-}33)$$

where the parameter η is usually chosen in the range $[10^{-8}, 10^{-5}]$ such that the truncation error is reduced.

To illustrate the use of the FDM, consider a slender column, subjected to a compression load, as shown in Figure 3.1(a). The idea is to compute the eigenvalue buckling sensitivity with respect to the design variables $\boldsymbol{x}$ in each element. The geometry, loading and boundary conditions are also given in Figure 3.1(a), and the other numerical values are: $E = 1$, $v = 0.3$, $P = 0.5$, $h = 1$, $t = 1$ (thickness), and $L = 12$.

For our problem, if $F = \lambda$ and $\boldsymbol{x} = \boldsymbol{E}$, from the Equation (3.32), we have:

$$\frac{\Delta\lambda}{\Delta E_j} = \frac{\lambda\left(\boldsymbol{E} + \Delta E_j \boldsymbol{e}_j\right) - \lambda(\boldsymbol{E})}{\Delta E} \qquad (3\text{-}34)$$

where:

$$\Delta E_j = \eta E_j \qquad (3\text{-}35)$$

Figure 3.1(b) and (c) show the finite element mesh using 2,000 polygonal elements and the corresponding first buckling mode, respectively.

Figure 3.2 illustrates a detail of the upper left corner of the column, where one concentrated load is applied. Figure 3.3 shows a comparison between the FDM and DDM methods, considering different values of η (see Equation (3-36)), for computing the sensitivity $\Delta\lambda_1/\Delta E_A$ with respect to the polygonal element shown in Figure 3.2. Finally, several contour plots of the sensitivities obtained by the FDM, considering values of η in the range $[10^{-10}, 10^{-1}]$, are illustrated in Figure 3.3. Note that for the range $[10^{-10}, 10^{-6}]$) we can get incorrect results,

which means that we need to adjust this parameter. Figure 3.3 shows that in the range $[10^{-5}, 10^{-1}]$) the solution is correct comparing to the DDM.

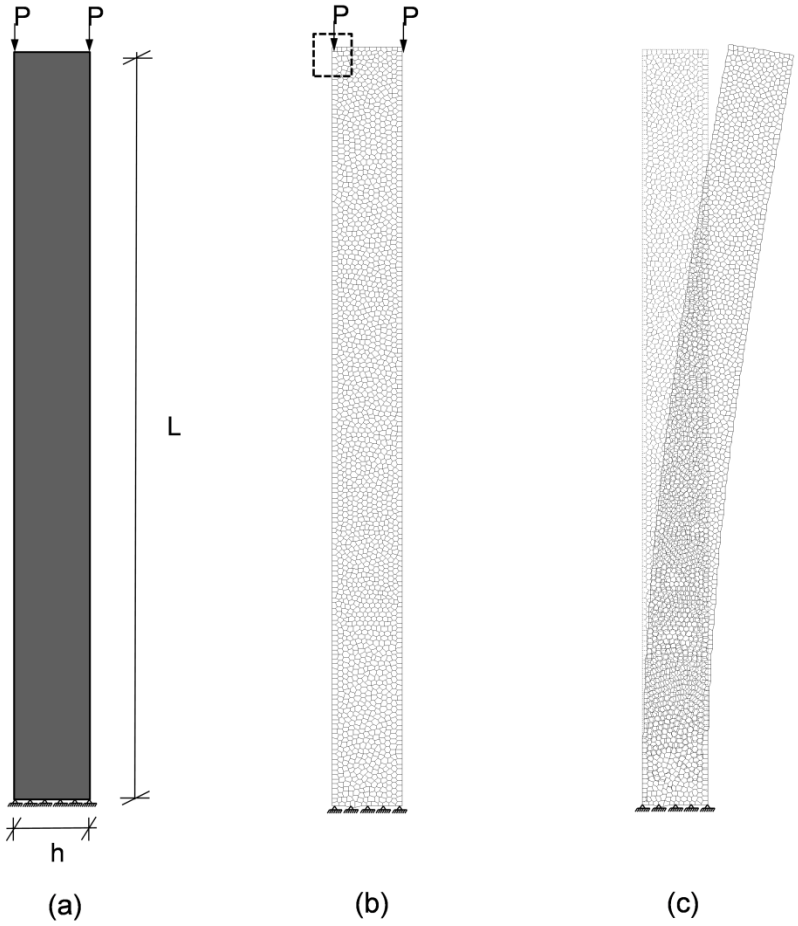

Figure 3.1: (a) Geometry, loading and boundary conditions, (b) finite element mesh using 2,000 polygonal elements, and (c) first buckling mode.

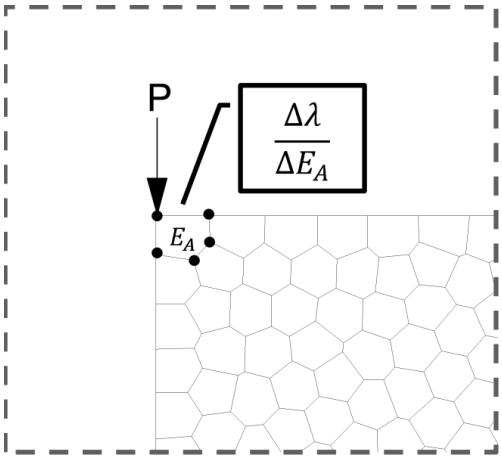

Figure 3.2: Detail shown in Figure 3.1(b).

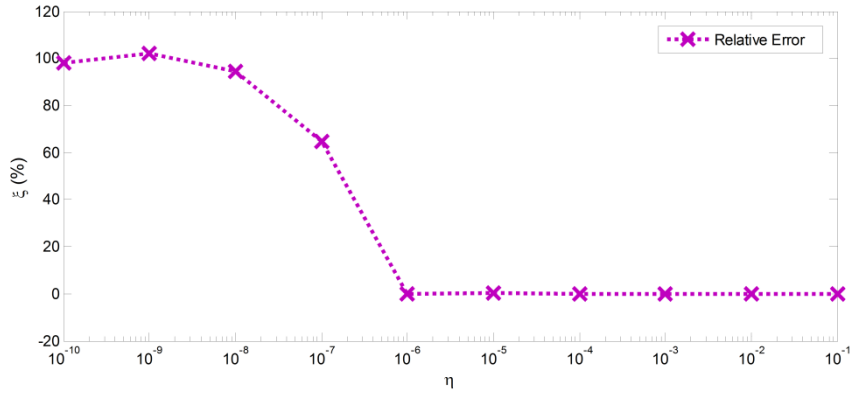

Figure 3.3: Relative Error (%).

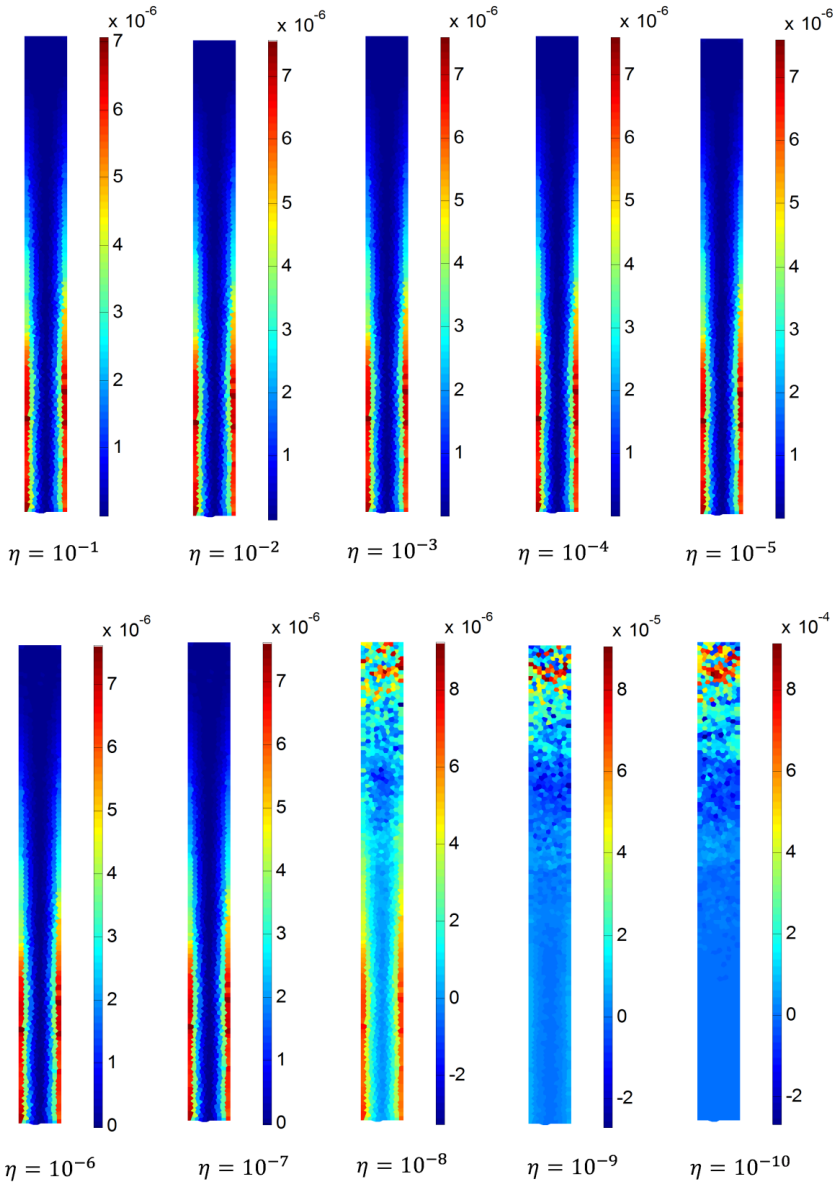

Figure 3.4 Contour plots of the eigenvalue buckling sensitivity for different values of the perturbation.

3.5
CPU Time Comparison

In this Section we use a representative example to compute the eigenvalue buckling sensitivities using the FDM, DDM, and AM methods. The results obtained here are compared with respect to the computational time.

The problem consists of a slender column subjected to an uniform compression. The geometry, loading and boundary conditions are illustrated in Figure 3.5(a), using quadrilateral elements, and Figure 3.7(a), using polygonal elements. The other numerical values used are: $E = 1 \times 10^7$, $v = 0.3, p = 1$, $h = 1$, $t = 1$ (thickness), and $L = 12$. The eigenvalue buckling sensitivities, with respect to the design variable x in each element, are computed.

For the simulations, we used an Intel Core i7-4930K CPU @ 3.40 GHz, with 64 GB of RAM, and the Microsoft Windows 7 64-bit operating system.

In our tests, we computed the sensitivities for different levels of mesh refinement. The results are shown in Figure 3.6 and Figure 3.8, for quads and polygons, respectively. Notice that the computational time with respect to the size of the problem grows quadratically, for the DDM, and linearly, for the AM. Finally, a comparison between the FDM, DDM and AM methods is shown in Figure 3.9, where we can observe that the computational time related to the FDM grows exponentially with respect to the size of the problem.

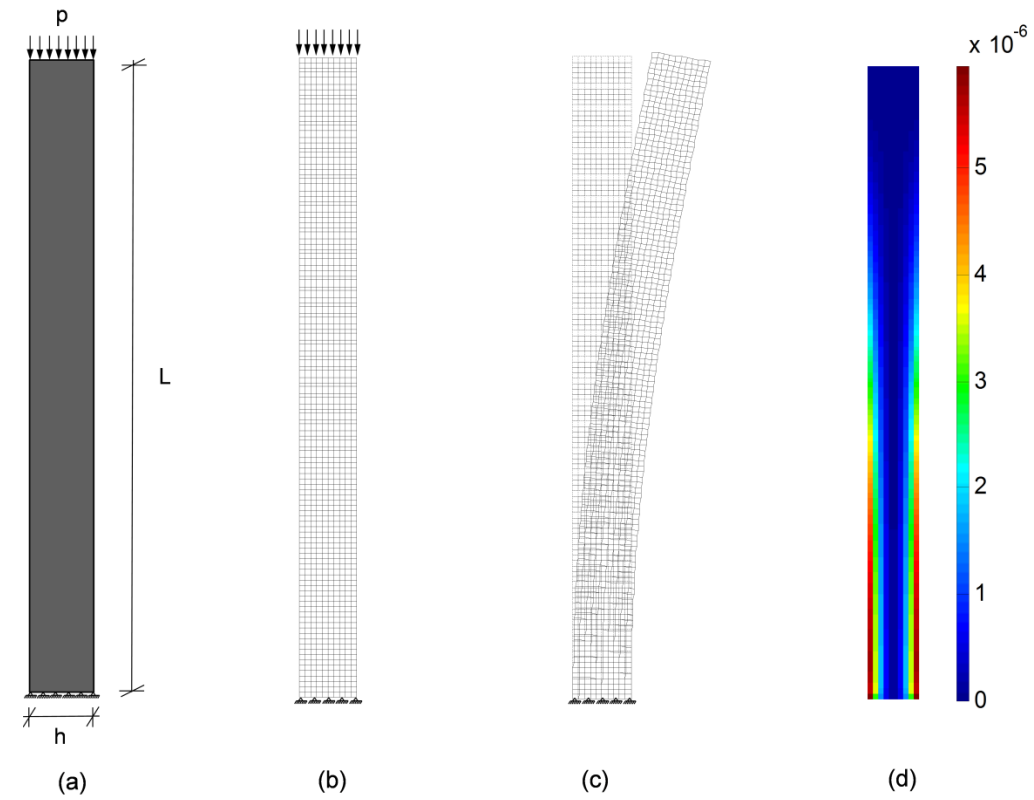

Figure 3.5: (a) Geometry, loading and boundary conditions for a column domain, (b) Discretization using 1,200 quad meshes; (c) First buckling mode and (d) contour plot of eigenvalue sensitivities.

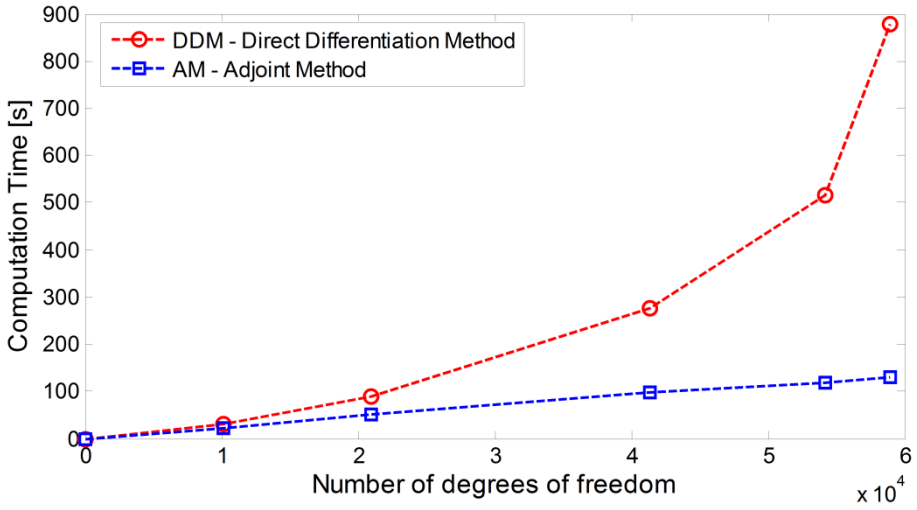

Figure 3.6: Computational time for the DDM and AM to compute the eigenvalue sensitivities, using Q4 (quadrilateral elements).

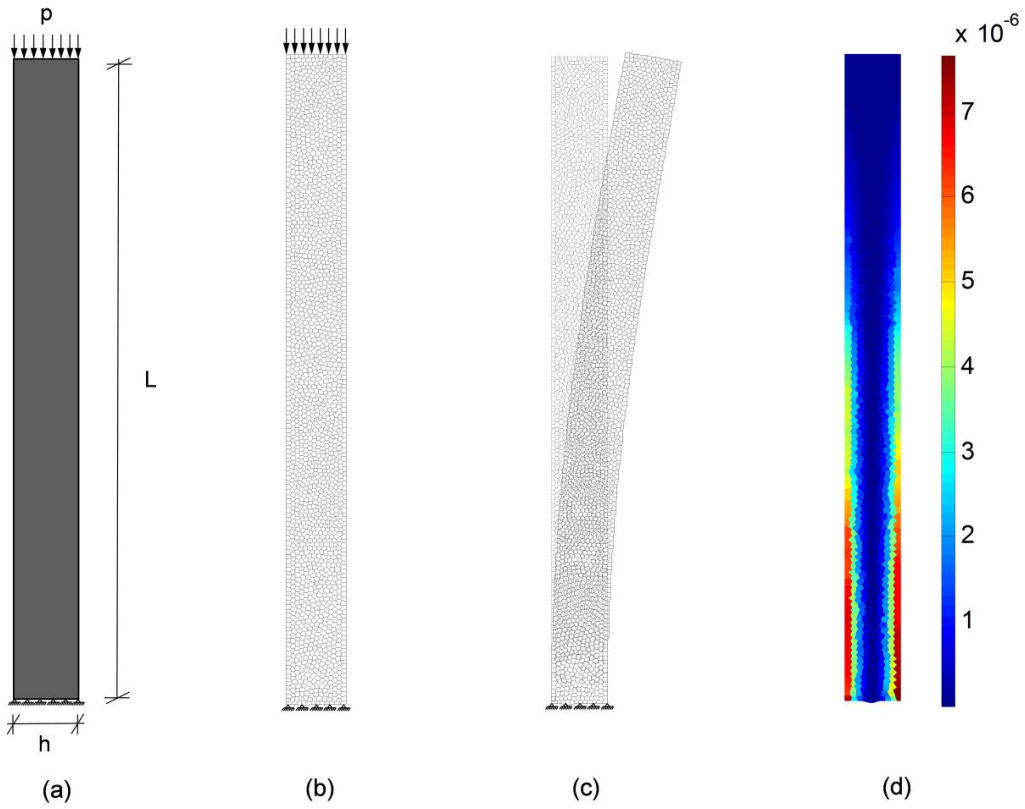

Figure 3.7: (a) Geometry, loading and boundary conditions for a column domain, (b) Discretization using 1,000 polygonal elements; (c) First buckling mode, and (d) Contour plot of eigenvalue sensitivities.

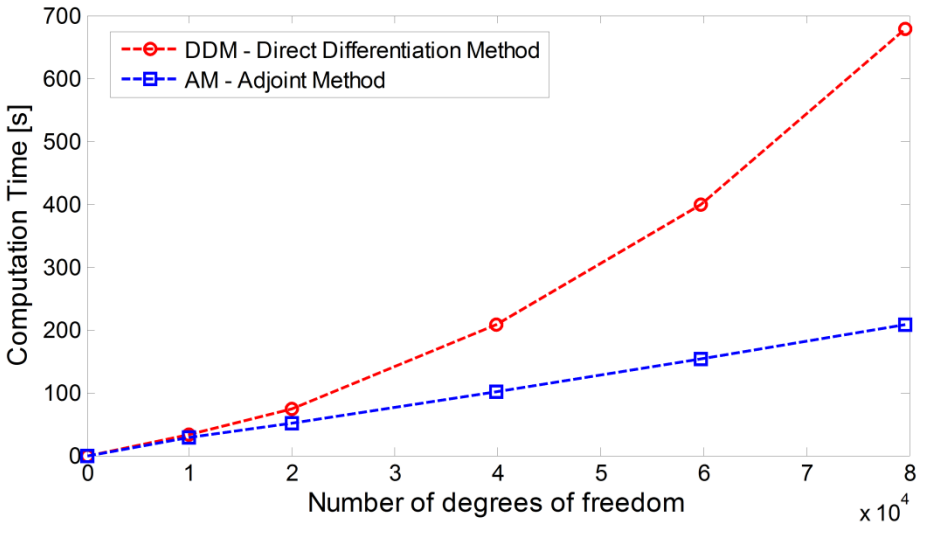

Figure 3.8: Computational time for the DDM and AM to compute the eigenvalue sensitivities, using polygonal elements.

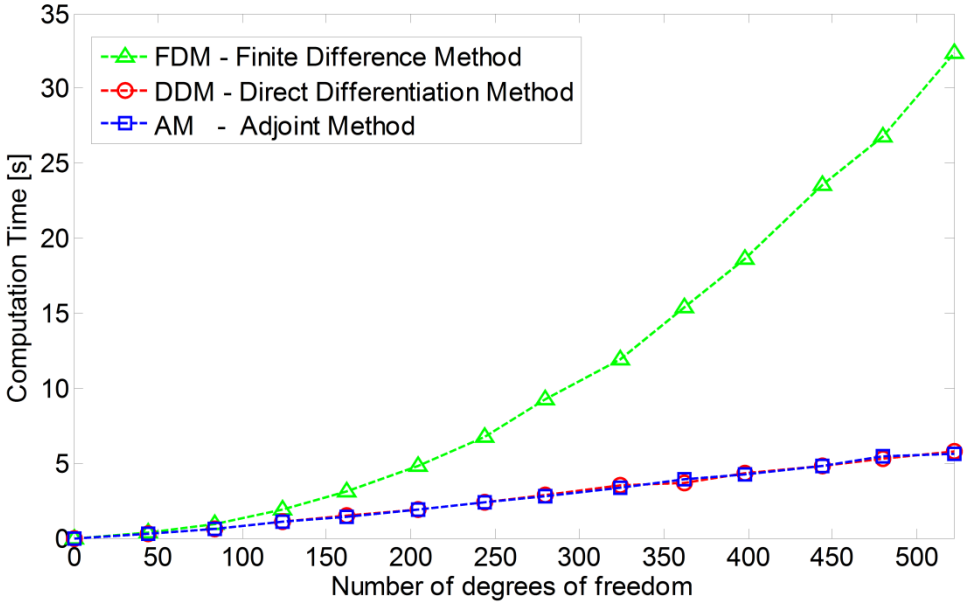

Figure 3.9: Computational time for the FDM, DDM and AM to compute the eigenvalue sensitivities using polygonal elements.

4.
Eigenvalue Topology Optimization

In this Chapter, we discuss the eigenvalue topology optimization problem. In Section 4.1 we show the problem of maximization of the first natural frequency, and in Section 4.2 we describe the problem of maximization of the first buckling load.

4.1.
Natural Frequency Optimization

The optimization problem corresponding to the eigenfrequency maximization can be expressed as the following $min - max$ problem:

$$\begin{cases} \max\limits_{x(\rho)} \quad \left\{\lambda_{min} = \min\limits_{j=1,\dots,N_{dof}} \{\omega_j^2\}\right\} \\ \text{s.t:} \\ \sum_{e=1}^{N_{el}} V_e\,\rho_e \leq V_s \\ \text{with:} \\ \boldsymbol{K}\boldsymbol{v}_j - \omega_j^2 \boldsymbol{M}\boldsymbol{v}_j = 0 \quad , \quad j = 1, \dots, N_{dof} \\ \text{and} \\ 0 < \rho_{min} \leq \rho_e \leq 1, \quad e = 1, \dots, N_{el} \end{cases} \qquad (4\text{-}1)$$

Here, λ_j is the j_{th} eigenfrequency, $\boldsymbol{v}_j$ is the corresponding eigenvector, and $\boldsymbol{K}$ and $\boldsymbol{M}$ are, respectively, the symmetric and positive definite stiffness and mass matrices associated to the finite element method. The eigenvalues, which are real and positive numbers, can be ordered as: $\omega_1^2 \leq \omega_2^2 \leq, \dots, \leq \omega_{N_{dof}}^2$ and the corresponding eigenvectors are $\boldsymbol{M}$-orthonormalized, $V_e\rho_e$ is the volume of each element and V_s is the upper bound on the final volume of the structure, defined by the user.

4.2
Buckling Optimization

For the buckling optimization problem the idea is to maximize the minimum critical buckling load λ. Considering only linear behavior, *i.e.,* for small displacements, the objective is to maximize the minimum critical load P_{crit}.

The optimization problem can be expressed as:

$$\begin{cases} \max\limits_{x(\rho)} \quad \left\{\lambda_{min} = \min\limits_{j=1,\dots,N_{dof}} \left\{P_{crit_j}\right\}\right\} \\ \text{s.t.:} \\ \sum_{e=1}^{N_{el}} V_e\,\rho_e \leq V_s \\ \text{with:} \\ \boldsymbol{K}\boldsymbol{u} = \boldsymbol{f} \\ \boldsymbol{K}\boldsymbol{v}_j + P_{crit_j}\boldsymbol{K}_\sigma\boldsymbol{v}_j = 0 \quad , \; j = 1, \dots, N_{dof} \\ \text{and} \\ 0 < \rho_{min} \leq \rho_e \leq 1, \;\; e = 1, \dots, N_{el} \end{cases} \tag{4-2}$$

Here, the eigenvalue λ_j corresponds to the j_{th} critical buckling load, $\boldsymbol{v}_j$ is the corresponding eigenvector (or buckling mode shape), and $\boldsymbol{K}$ and $\boldsymbol{K}_\sigma$ are, respectively, the symmetric and positive definite elastic and geometric (or stress) stiffness matrices associated to the finite element method (M. P. Bendsøe et al. [14]). The eigenvalues, which are real and positive numbers, can be ordered as: $\lambda_1 \leq \lambda_2 \leq, \dots, \leq \lambda_{N_{dof}}$ and the corresponding eigenvectors are $\boldsymbol{K}_\sigma$-orthonormalized, $V_e\rho_e$ is the volume of each element and V_s is the upper bound on the final volume, defined by the user.

4.3
Formulation: Objective and Volume Constraint Functions

The SIMP (Solid Isotropic Material with Penalization) model proposed by M. P. Bendsøe et al. [14], [38] is a simple and effective material model that is widely used to achieve optimum topology designs. The model is usually applied together with a filter technique, in order to prevent checkerboard formation and a dependency of optimum topology solutions on the finite element mesh refinement.

From the article by F. Evqueni et al. [39], the density of the element ρ_i is computed based on the weighted average of the nearby design variable as:

$$\rho_i = \frac{\sum_{n \in S_i} \bar{y}\, w(x_n - x_i)}{\sum_{n \in S_i} w(x_n - x_i)} \qquad (4\text{-}3)$$

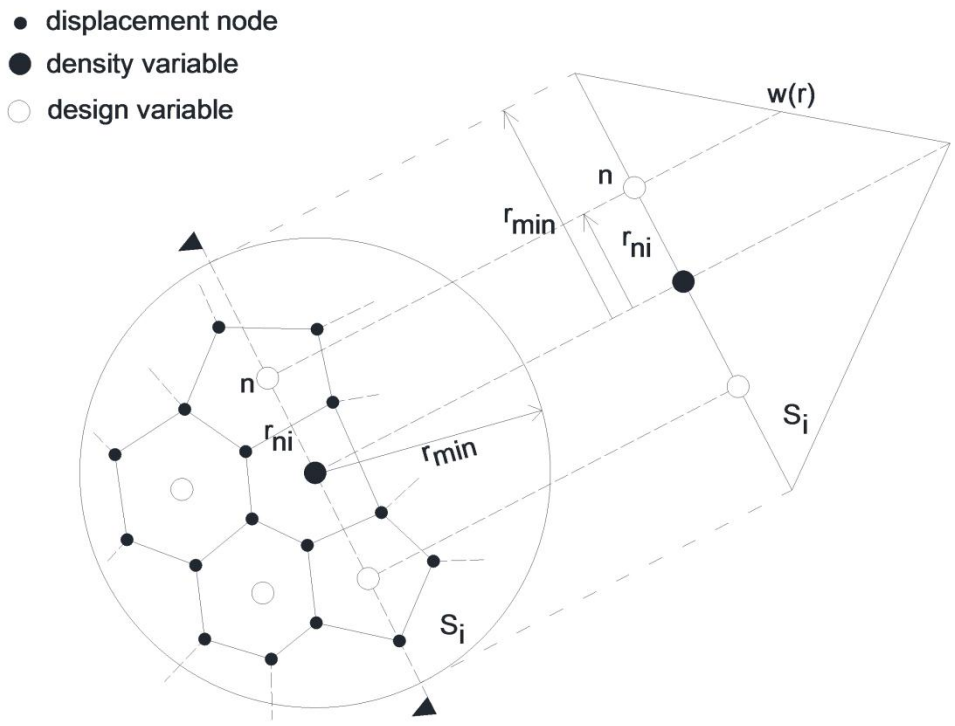

Figure 4.1: Projection scheme from the design variables to the element density.

Here, S_i is the sub-domain corresponding to the density element, x_n is the position of the centroid of the design variable $\bar{y}$. The weight function for this linear approach can be defined as:

$$w(x_n - x_i) = \begin{cases} \frac{r_{min} - r_{ni}}{r_{ni}} & if\ r_{ni} \leq r_{min} \\ 0 & otherwise \end{cases} \quad (4\text{-}4)$$

where r_{ni} is the distance between the centroid of the density element i and the design variable $\bar{y}$, and r_{min} is the length scale of the filter defined by the user (See Figure 4.1). The sensitivities of the element density with respect to the design variables are obtained as:

$$\frac{\partial \rho_i}{\partial \bar{y}} = \frac{w(x_n - x_i)}{\sum_{m \in S_i} w(x_m - x_i)} \quad (4\text{-}5)$$

The projection operator is written in matrix form $\boldsymbol{P}$ as:

$$\boldsymbol{y} = \boldsymbol{P}\boldsymbol{z} \quad (4\text{-}6)$$

Then, we define vectors m_E, m_m, and m_σ as material interpolation functions, *i.e.*:

$$\boldsymbol{E} := m_E(\boldsymbol{y}) \quad (4\text{-}7)$$

$$\boldsymbol{E}_m := m_m(\boldsymbol{y}) \quad (4\text{-}8)$$

$$\boldsymbol{E}_\sigma := m_\sigma(\boldsymbol{y}) \quad (4\text{-}9)$$

$$\boldsymbol{V} := m_V(\boldsymbol{y}) \quad (4\text{-}10)$$

where in the case of SIMP, we have:

$$\bar{E}(y) = \varepsilon + (1 - \varepsilon)\bar{y}^p \quad (4\text{-}11)$$

$$\bar{E}_m(y) = \bar{y}^q \quad (4\text{-}12)$$

$$\bar{E}_\sigma(y) = \bar{y}^g \quad (4\text{-}13)$$

Here, p, q, and g are the respective penalization factors and ε is the Ersatz number. Thus, the corresponding elastic, geometric, and mass matrices are given as:

$$\boldsymbol{K} = \sum_{e=1}^{N_{el}} m_E(y_e)\boldsymbol{k}^e, \quad (4\text{-}14)$$

$$\boldsymbol{K}_\sigma = \sum_{e=1}^{N_{el}} m_\sigma(y_e)\boldsymbol{k}_\sigma^e, \text{ and} \quad (4\text{-}15)$$

$$\boldsymbol{M} = \sum_{e=1}^{N_{el}} m_m(y_e)\boldsymbol{m}^e, \quad (4\text{-}16)$$

4.4. Optimization Algorithm

The optimization algorithm is responsible for updating the design variables toward the optimal solution. Several algorithms, available in the literature, can be used for solving density-based topology optimization problems. Two of the most well known algorithms for this class of problems are the Optimality Criteria (OC) (see, for example, D. Gunwant and A. Misra [40]) and the Method of Moving Asymptotes (MMA), (developed by Svanberg K. [41]).

In this study, we solved the buckling topology optimization problem using the OC method. This method is very simple and can applied in optimization problems where there is only one constraint function (in this case, an upper bound on the final volume of the structure).

4.4.1 Optimality Criteria

The basic idea of this method consists of replacing the objective and constraint functions by suitable approximations in the neighborhood of the current design point. In other words, we solve the following approximate problem in each iteration:

$$\min_{\boldsymbol{z}^L \le \boldsymbol{z} \le \boldsymbol{z}^U} J(\boldsymbol{z}) \quad (4\text{-}17)$$

Here, $J(\boldsymbol{z})$ is an approximation to the objective function, and $\boldsymbol{z}^L$ and $\boldsymbol{z}^U$ specify the lower and upper bounds, respectively, for the search region where the approximation is valid. Denoting M as the admissible move limit and $\boldsymbol{z}^0$ as the design at the current iteration, we get:

$$z_l^L = \max\left(z_l^o - M, \underline{\rho}\right), \qquad l = 1, \dots, N \tag{4-18}$$

$$z_l^U = \min(z_l^o + M, \overline{\rho}), \qquad l = 1, \dots, N \tag{4-19}$$

where $\underline{\rho}$ and $\overline{\rho}$ specify the lower and upper bounds of the density.

Note that the function J can be written as:

$$J(\boldsymbol{z}) = f(\boldsymbol{z}) + \mu\, g(\boldsymbol{z}) \tag{4-20}$$

where f and g are the objective and constraint functions, respectively, which were obtained from the first order Taylor expansion.

To obtain the approximate function $J(\boldsymbol{z})$, the first term $f(\boldsymbol{z})$ is linearized in the exponential intermediate variables [42]:

$$\left(\frac{z_l - \underline{\rho}}{\overline{\rho} - \underline{\rho}}\right)^a \tag{4-21}$$

with $a \leq 1$, the current value of the design variable $\boldsymbol{z} = \boldsymbol{z}^0$, the first-order Taylor expansion in these intermediate variables yields:

$$f_{app}(\boldsymbol{z}) = f(\boldsymbol{z}^0) + \sum_{l=1}^{N} \frac{1}{a}\left(z_l^0 - \underline{\rho}\right)\left[\left(\frac{z_l - \underline{\rho}}{z_l^0 - \underline{\rho}}\right)^a - 1\right]\frac{\partial f}{\partial z_l}\bigg|_{\boldsymbol{z}=\boldsymbol{z}^0} \tag{4-22}$$

The constraint function is approximated linearly in the design variables:

$$g_{app}(\boldsymbol{z}) = g(\boldsymbol{z}^0) + \sum_{l=1}^{N} (z_l - z_l^o)\frac{\partial g}{\partial z_l}\bigg|_{\boldsymbol{z}=\boldsymbol{z}^0} \tag{4-23}$$

The condition of optimality provides the relationship between the Lagrange multiplier μ and each design variable z_l:

$$\nabla J(\boldsymbol{z}^*) = \frac{\partial f_{app}}{\partial z_l} + \mu \frac{\partial g_{app}}{\partial z_l} = 0\,, \qquad l = 1, \dots, N \tag{4-24}$$

The value of the Lagrange multiplier μ is obtained by solving the dual problem using a bi-section method.

By substituting Equation (4-22) and Equation (4-23) into Equation (4-24), we can obtain an explicit expression for z^*:

$$\left(\frac{z_l - \underline{\rho}}{z_l^o - \underline{\rho}}\right)^{1-a} = \frac{-\frac{\partial f}{\partial z_l}\Big|_{\boldsymbol{z}=\boldsymbol{z}_o}}{\mu \frac{\partial g}{\partial z_l}\Big|_{\boldsymbol{z}=\boldsymbol{z}_o}} = B_l \tag{4-25}$$

$$z_l^* = \underline{\rho} + B_l^{\frac{1}{1-a}}\left(z_l^o - \underline{\rho}\right), l = 1, \dots, N \tag{4-26}$$

where z_l^* is the candidate for the new iteration.

Using the convexity of $J(\boldsymbol{z})$, the minimizer $\boldsymbol{z}^{new}$ is given by:

$$z_l^{new} = \begin{cases} z_l^U, & z_l^* \le z_l^U \\ z_l^L, & z_l^* \ge z_l^L \\ z_l^*, & otherwise \end{cases}, l = 1, \dots, N \tag{4-27}$$

or by:

$$z^L = \max(z_l^o - M, \underline{\rho}) \tag{4-28}$$

$$z^U = \min(z_l^o + M, \overline{\rho}) \tag{4-29}$$

$$z_l^{new} = \max(\max(\min(\min(\, z_l^*, z_l^o + M), \overline{\rho}), z_l^o - M), \underline{\rho}) \tag{4-30}$$

The update scheme consisting of Equation (4-30) is commonly known as the OC method, and the quantity $\varsigma = \frac{1}{1-a}$ is sometimes referred to as the damping coefficient. For the so-called reciprocal approximation, $a = -1$, and thus $\varsigma = \frac{1}{2}$ (for more details, see Talischi *et al.,* [32], [39].)

4.5.
Spurious Localized Buckling Mode

During the numerical optimization process, a common problem, known as spurious mode or local mode, is often observed. This is because of the low density of some elements in the mesh (void areas).

According to Browne [6], Pedersen [43] and Neves *et al.* [15], a low-density element is defined as one where the density is below a certain threshold, which is usually taken as 10% of the initial density value. As an example, consider the problem studied by Browne P. [6], which is shown in Figure 4.2. A square domain ($L = t = 10\,m$) discretized with 10×10 quadrilateral elements is subjected to a vertical concentrated load ($P = 1\,N$) pointing downwards, which is applied at the top of the design domain; the base is considered fixed. The material properties are $E = 1\,N/m^2$ and $v = 0.3$. The Ersatz parameter is taken as $eps = 10^{-9}$, and we used a filter with a radius of $R = 0.04\,m$. The objective is to minimize the compliance of the structure with a constraint on the volume corresponding to 20% of the initial volume, and a penalization factor $p = 4$ is applied on the stiffness matrix. This problem is solved here using the *SIMP* model together with the *OC* optimizer.

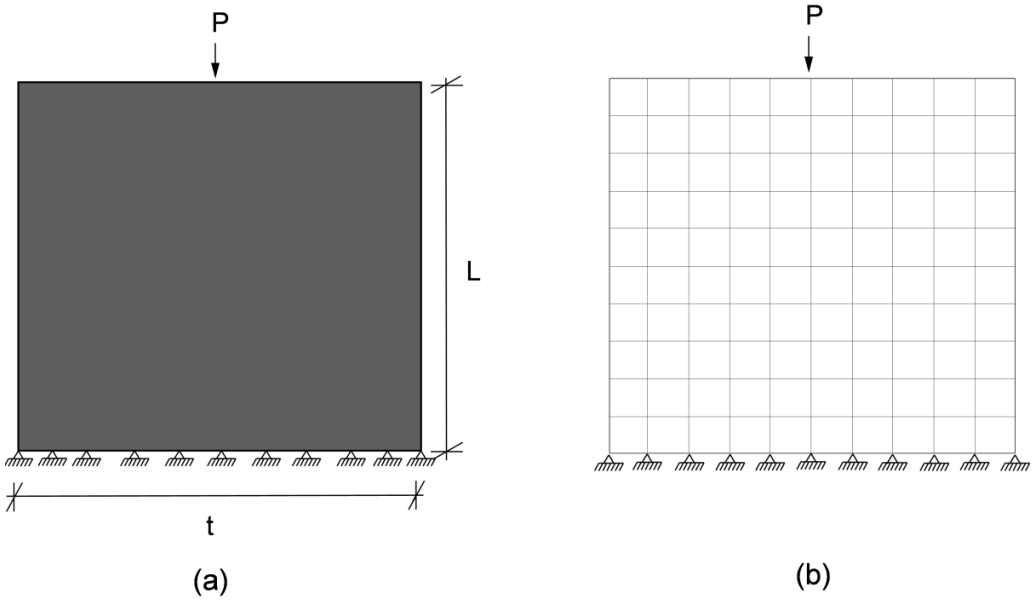

Figure 4.2: (a) Geometry, loading and boundary conditions. (b) Finite element mesh using *10×10* quadrilateral elements.

Figure 4.3 and Figure 4.4 show the material distribution inside the domain after iterations 1, 7 and 10, respectively, of the topology optimization process for compliance minimization. For each material distribution, we computed the first linearized buckling load and corresponding buckling mode.

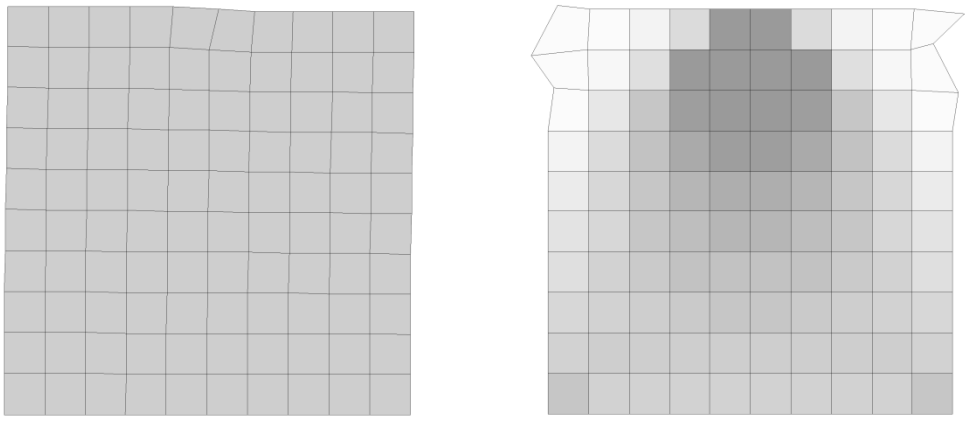

(a) (b)

Figure 4.3: (a) Initial distribution of material and corresponding mode shape; (b) Distribution of material and corresponding mode shape after 1 iteration.

Figure 4.3(a) shows the first ocurrence of spurious buckling modes. The elements in the top corners are the first to get to a low value of density and we can see that in these areas the buckling mode is localized (see Figure 4.3 (b)). This is the first time that the element density drops below 0.1, which is the critical value pointed out by Pedersen [43] and Neves *et al.* [15].

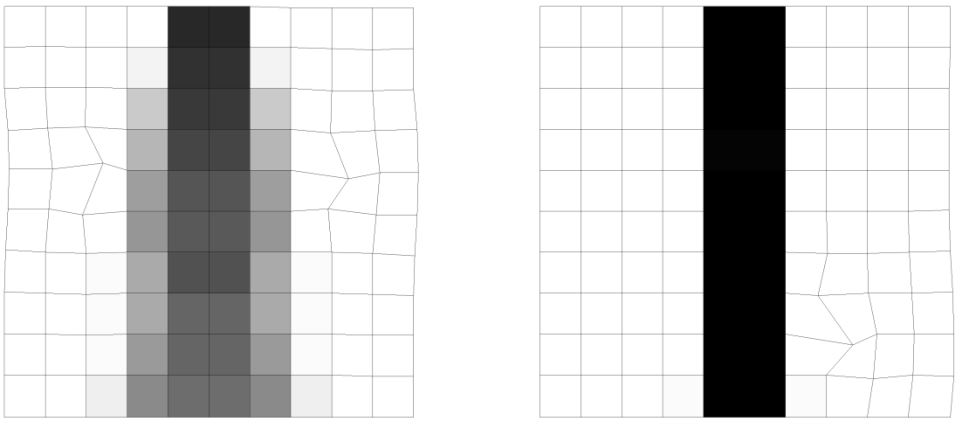

(a) (b)

Figure 4.4: Distribution of material and corresponding mode shape; (a) after 7 iterations; (b) after 10 iterations.

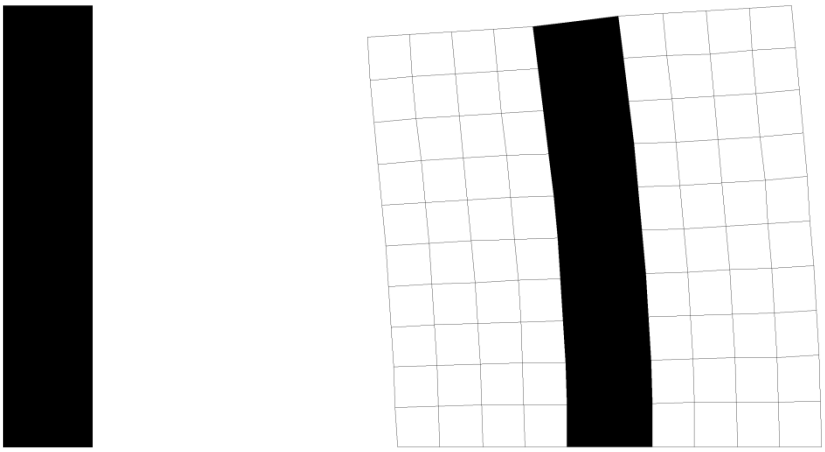

(a) (b)

Figure 4.5: (a) Final distribution of material. (b) Mode shape corresponding to the 19th smallest positive eigenvalue.

The mode shape shown in Figure 4.4(b) corresponds to the smallest positive eigenvalue at the final solution of the optimization problem. However, the buckling mode associated with the smallest positive eigenvalue may not correspond to the desired mode shape, as illustrated in Figure 4.5(b), where the desired mode shape is associated with the 19th smallest positive eigenvalue.

To avoid this problem, we followed the suggestion proposed by Bendsøe and Sigmund [14], and used by Boom, S. [18], which consists of using different values of the penalization factor for the elastic ($\boldsymbol{K}$) and geometric ($\boldsymbol{K}_\sigma$) stiffness matrices. The basic idea here is to penalize $\boldsymbol{K}_\sigma$ because low-density elements do not contribute to the geometric stiffness matrix. According to Boom, S. [18], another advantage of this strategy is that it makes the geometric stiffness matrix a continuous and differentiable function of the element densities, which is very important when gradient-based optimization methods are used. Let p and g be the penalization factors for $\boldsymbol{K}$ and $\boldsymbol{K}_\sigma$, respectively. The buckling of void elements is prevented when $p < g$.

To illustrate this strategy, consider the example shown in Figure 4.6. A square domain ($L = t = 10m$) is discretized with $6x6$ quadrilateral elements, subjected to a vertical load ($P = 1N$) pointing downwards, and applied at the top of the design domain; the base is considered fixed. The material properties are: $E = 1\ N/m^2$ and $\nu = 0.3$. The Ersatz parameter is taken as $eps = 10^{-9}$, and we used a filter with radius $R = 0.04\ m$. The objective is to maximize the eigenvalue

of the structure with a constraint on the volume corresponding to 65% of the initial volume. Variable values of p are used to penalize the elastic stiffness matrix and variable values of g, for the geometric stiffness matrix. This problem is solved here using the $SIMP$ model together with the OC optimizer. As expected, no buckling of the void elements is observed when $p < g$ as shown in Figure 4.7.

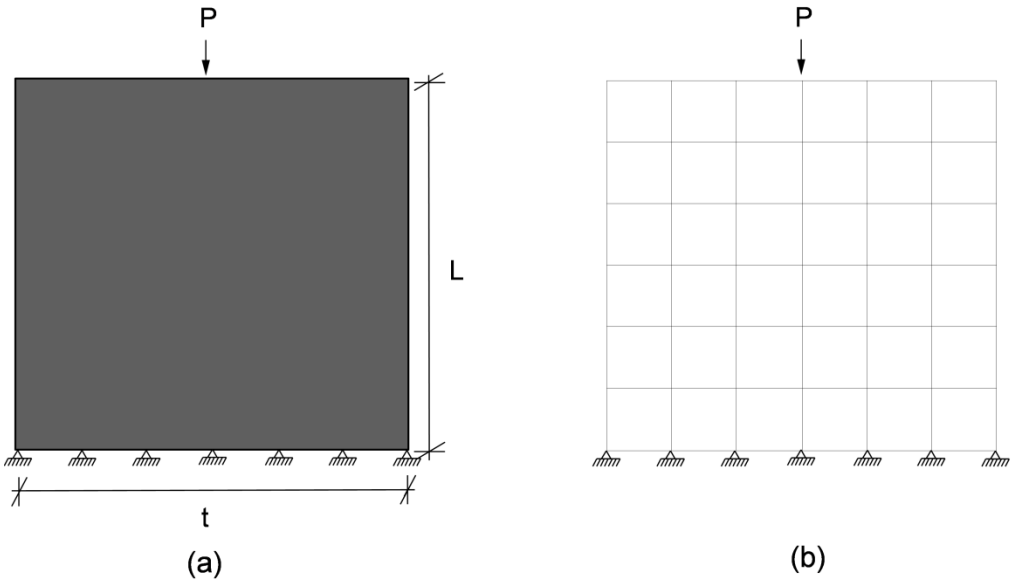

Figure 4.6: (a) Geometry, loading and boundary conditions. (b) Finite element mesh using *6×6* quadrilateral elements.

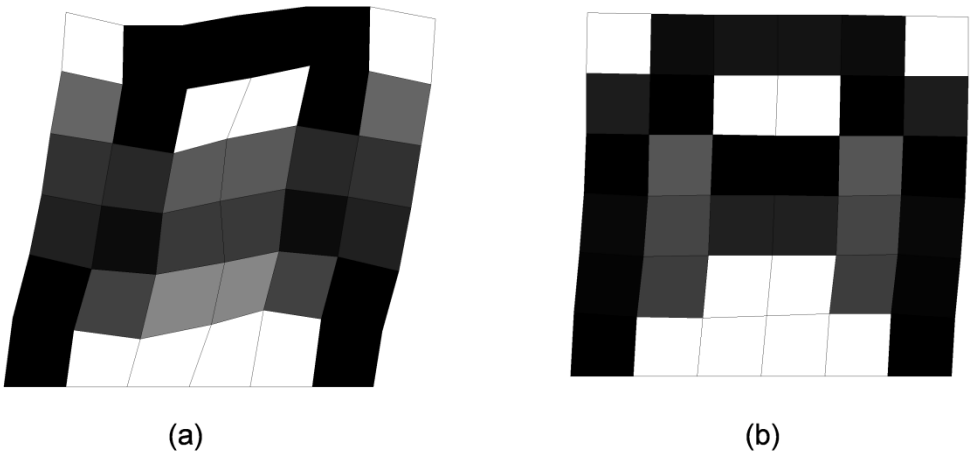

Figure 4.7: First buckling mode for (a) $p > g$ and (b) $p < g$.

A similar example, illustrated in Figure 4.8, is studied here for the eigenfrequency problem. It consists of a square domain ($L = t = 10\,m$) discretized with $6x6$ quadrilateral elements; and supported-supported boundary condition. The material properties are: $E = 1\,N/m^2$ and $\nu = 0.3$. The Ersatz

parameter is taken as $eps = 10^{-9}$, and we used a filter with radius $R = 0.04\,m$. The objective is to maximize the first eigenvalue of the structure with a constraint on the volume corresponding to 60% of the initial volume. Variable values of p are used to penalize the elastic stiffness matrix and variable values of q, for the mass matrix. This problem is solved using the $SIMP$ model together with the OC optimizer. As expected, no buckling of the void elements is observed when $p < q$, as shown in Figure 4.9.

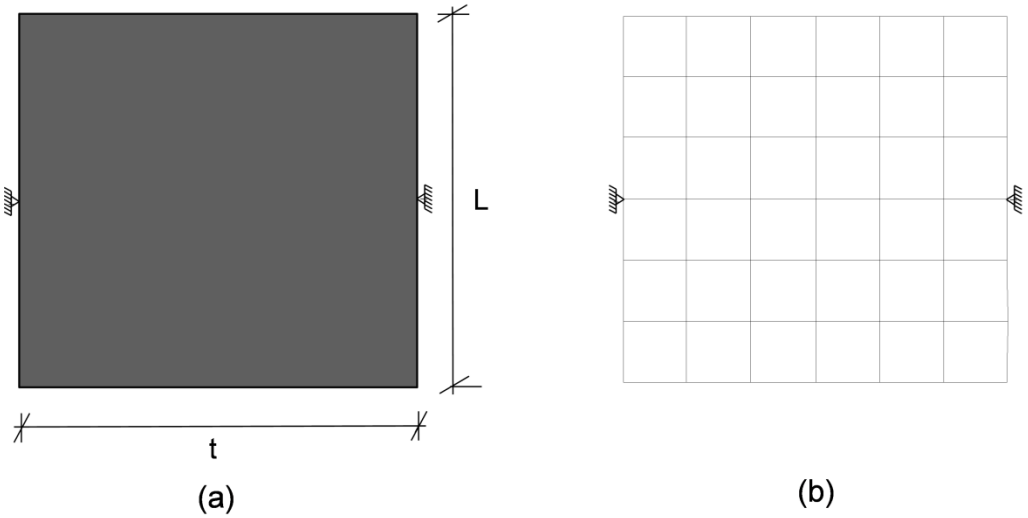

Figure 4.8: (a) Geometry, loading and boundary conditions. (b) Finite element mesh using *6×6* quadrilateral elements.

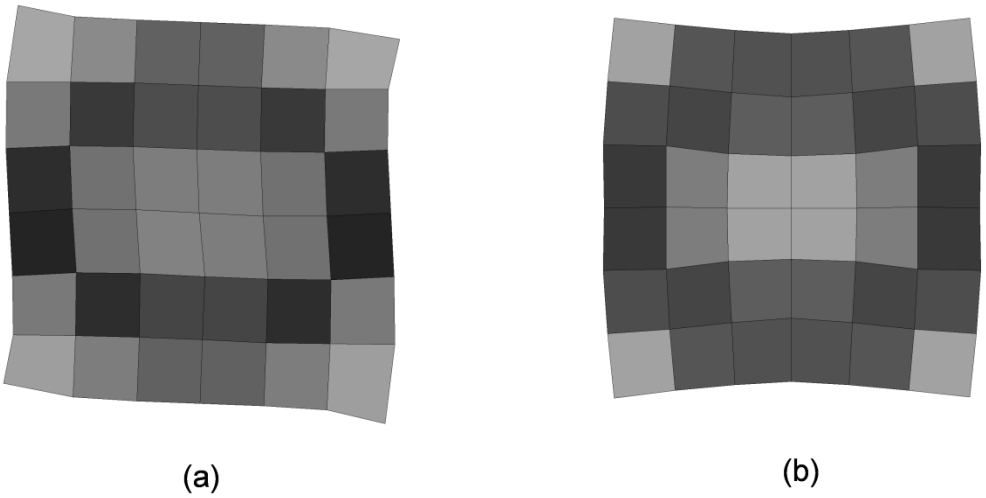

Figure 4.9: First shape mode for (a) $p > q$ and (b) $p < q$.

4.6.
Numerical Implementation

`PolyMesher` is a simple and robust MATLAB® code for polygonal mesh generation. The main ingredients of `PolyMesher` are the implicit representation of the domain and the use of Centroidal Voronoi diagrams for its discretization. The implicit description offer great flexibility to construct a relatively large class of domains with algebraic expressions. A discretization of the domain is constructed from a Centroidal Voronoi tessellation (CVT) that incorporates an approximation to its boundary. This approximation is obtained by including the set of reflections of the seeds. Additionally, Lloyd's method is used to establish a uniform (optimal) distribution of seeds and thus a high quality mesh (for more details, see reference [7]). Figure 4.10 shows some iterations of the Lloyd's method.

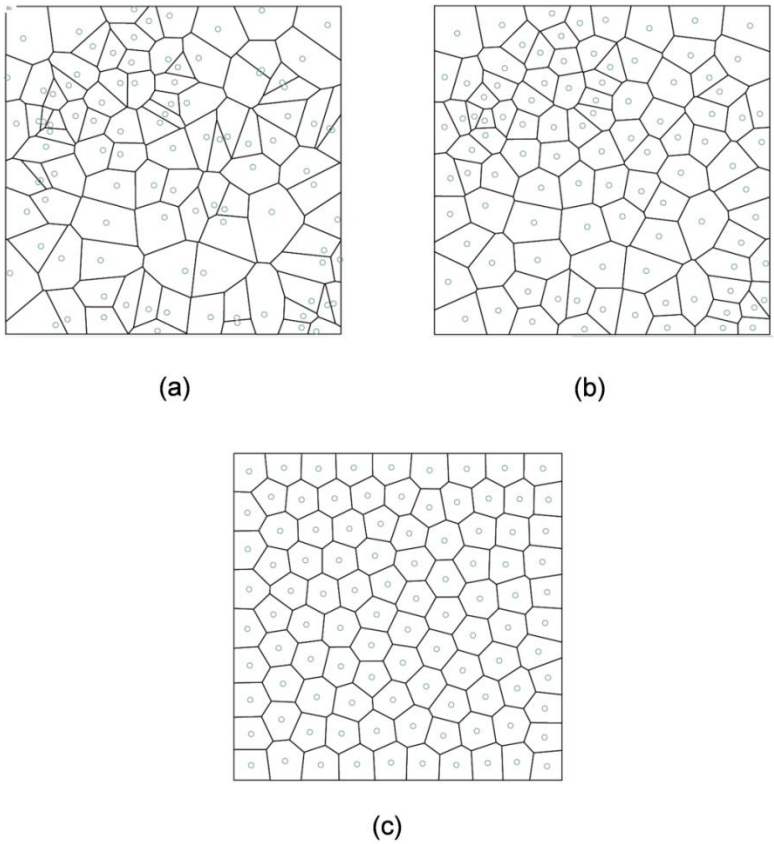

Figure 4.10: Lloyd's method. (a) Initial random distribution of seeds and corresponding Voronoi diagram; (b) First iteration; (c) Distribution of seeds after 80 iterations.

To generate a mesh using `Polymesher` the user needs to provide the following informations: the domain function (*e.g. MbbDomain*, *MichellDomain, etc.*) maximum number of Lloyd's iterations (`MaxIter`), and number of polygonal elements (`NElem`). The command line to call the `Polymesher` function is the following:

```
[Node,Element,Supp,Load]=Polymesher[@Domain,NElem,MaxIter]
```

The corresponding output data are: `Node`, a vector with the coordinates of all nodes in the mesh; `Element`, a cell array containing the connectivity of each polygonal element, `Supp` and `Load` are vectors containing boundary conditions and load values, respectively. (More details about this function can be found in the work by Talischi *et al.* [8]).

`Polytop` is an efficient code developed in MATLAB® for structural topology optimization that includes a general finite elemens routine based on isoparametric polygonal elements. According to the authors [32], the code also features a modular structure in which the analysis routine and the optimization algorithm are separated from the specific choice of topology optimization formulation.

Within this framework, finite element and sensitivity analysis routines were modified, where:

`FEAnalysis`, contain formulations to solve eigenvalue problem.

`ObjectiveFnc`, objective function (e.g. eigenvalue) and `ConstraintFnc`, constraint function (e.g. volume fraction) are used during the sensitivity analysis. Note that other formulations can be used and thus the code can be extended, developed and modified independently, according to the new type of problem.

The variables are updated in the `UpdateScheme` routine using optimality criterion method OC as the optimizer algorithm. More details about the code can be found in Reference [32].

The main steps required to achieve an optimal topology for a linearized critical buckling load problem are illustrated in the flowchart depicted in Figure 4.11.

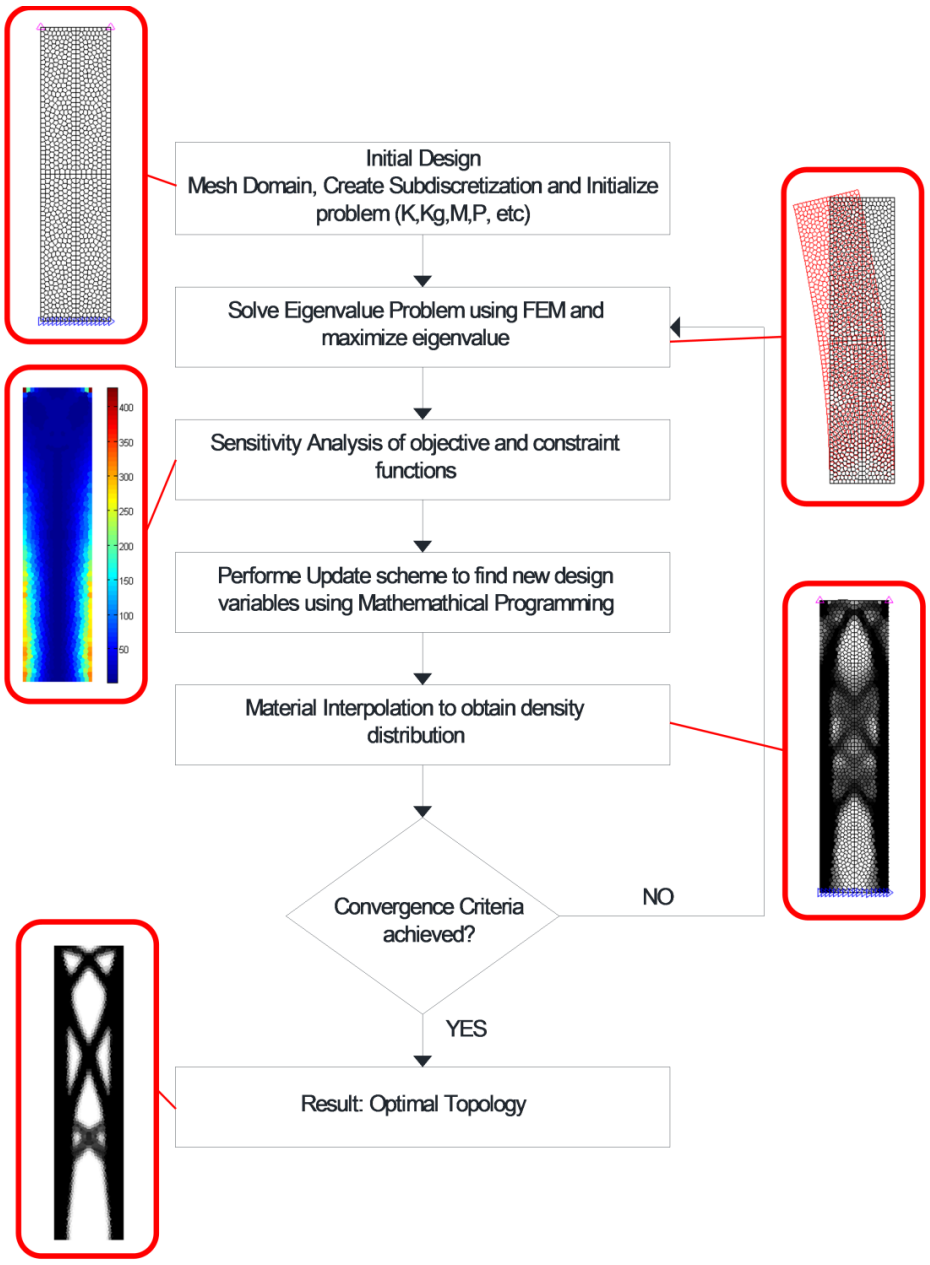

Figure 4.11: Flowchart for topology optimization applied to an eigenvalue problem.

5.
Results and Discussion

5.1.
Topology optimization for eigenfrequency problems

The beams shown in Figure 5.1(a), Figure 5.6(a) and Figure 5.9(a) are considered here to maximize their fundamental frequency. The main input parameters are: $L = 8\,m$, $h = 1\,m$, $E = 10^7\ N/m^2$, $\upsilon = 0.3$, and the initial material density $\rho = 0.5$. The beam domain is discretized with $10{,}000$ polygonal elements, and the volume fraction of 50%, which defines the upper bound on the final volume (V_s) of the structure. The OC algorithm is used as the optimization algorithm. The results obtained here to maximize the fundamental frequency are illustrated in Figure 5.1 to Figure 5.8. This example was also studied by J. Du and N. Olhoff [29], and their final topology is shown in Figure 5.1(d), Figure 5.6(d) and Figure 5.9(d). Three boundary conditions are considered: simply supported; clamped–clamped; and clamped–supported.

5.1.1
Simply Supported Beam

Figure 5.1(a) and Figure 5.1(b) show, respectively, a simply supported beam and the corresponding polygonal finite element mesh. The final topology obtained for maximizing the fundamental eigenfrequency is illustrated in Figure 5.1(c). We adopted $p = 4$ for penalizing the elastic stiffness matrix and $q = 0.5$ for the mass matrix. Optimal design obtained by J. Du and N. Olhoff [29] is shown in Figure 5.1(d).

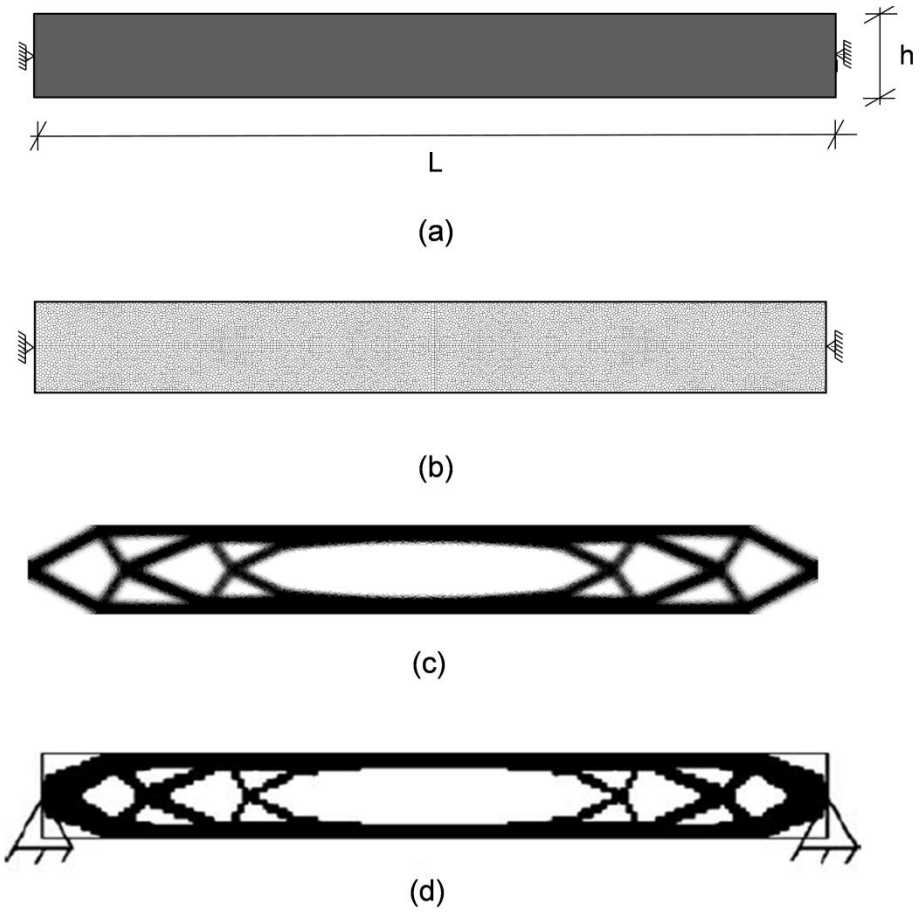

Figure 5.1: Simply supported beam: (a) Geometry and boundary conditions; (b) Polygonal finite element mesh; (c) Optimal topology obtained in this study (d) Optimal topology obtained by [29], when 1st eigenfrequency is maximized.

Figure 5.2(a) illustrates the convergence of the objective function (*i.e.* the fundamental eigenfrequency) and the next two eigenfrequencies with respect to the number of iterations. Figure 5.2(b) shows the results obtained by J. Du and N. Olhoff [29].

It is important to mention that, in this example, the multiplicity of eigenfrequencies (first and second) can be found because we compute the sensitivity of a single eigenvalue. Therefore, when maximizing the first eigenvalue, the sensitivity affects only this single eigenvalue and the second and third ones may decrease during the optimization process.

To overcome this problem, we can compute the sensitivity for repeated eigenvalues, using a linear combination of eigenvalues (see, for example, the work by R. Mosmann [44] and C. Guilherme [45]). Here, we only compute the sensitivity for a single eigenvalue.

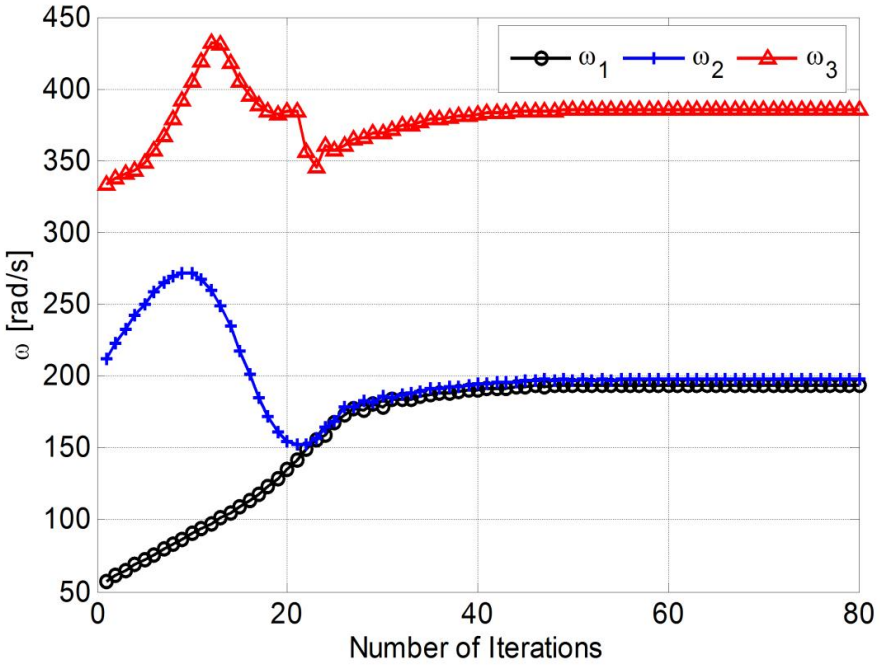

(a)

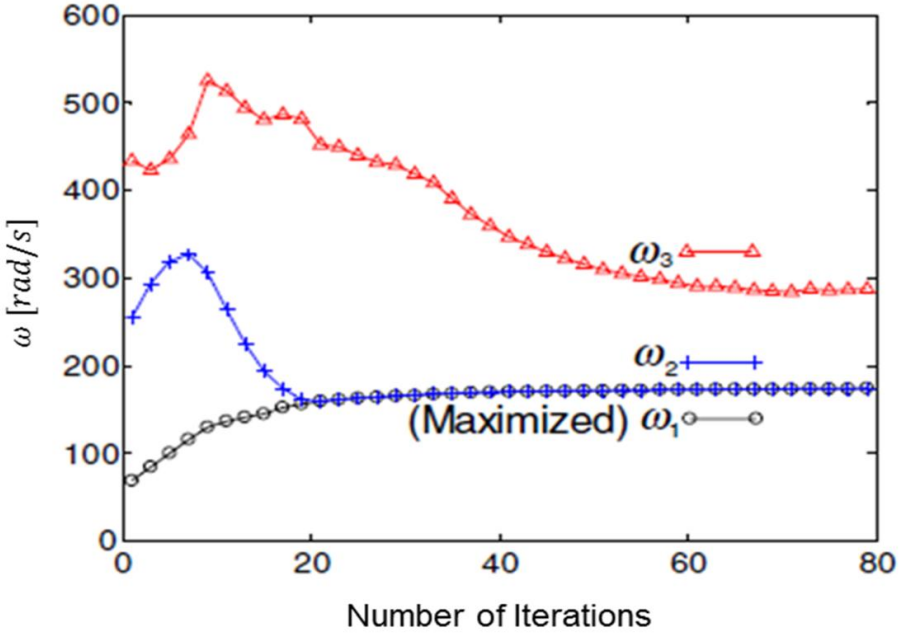

(b)

Figure 5.2: Simply supported beam: (a) Convergence of the first three eigenfrequencies (b) Results obtained by [29].

The final topologies and the respective mode shapes, for the simply supported case, are shown in Figure 5.3. The results obtained here are in good

agreement with the ones obtained by J. Du and N. Olhoff [29] and illustrated in Figure 5.4.

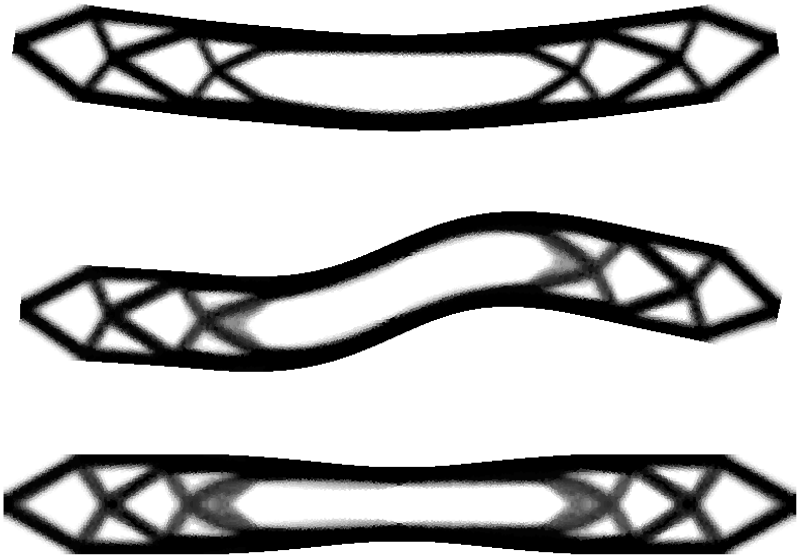

Figure 5.3: Simply supported beam: First three eigenmodes

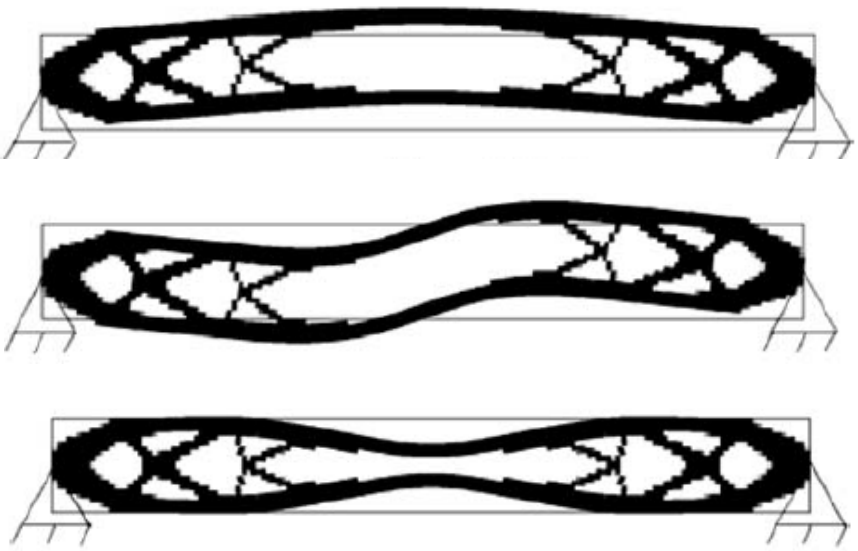

Figure 5.4: Simply supported beam: First three eigenmodes obtained by [29].

Finally, Figure 5.5(a) shows the optimal topology obtained when the second eigenfrequency is maximized, considering the simply supported case and

polygonal finite elements. Figure 5.5(b) shows the final topology obtained by J. Du and N. Olhoff [29].

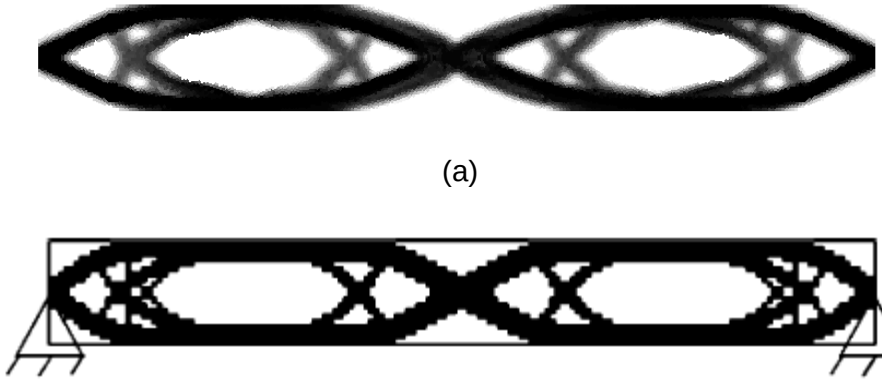

(a)

(b)

Figure 5.5: Simply supported beam: (a) Optimal topology obtained in this study for maximizing the second eigenfrequency (b) Optimal topology obtained by [29].

5.1.2
Clamped-Clamped Beam

Figure 5.6(a) and Figure 5.6(b) show, respectively, a clamped–clamped beam and the corresponding polygonal finite element mesh. The final topology obtained for maximizing the fundamental eigenfrequency is illustrated in Figure 5.6(c). We adopted $p = 8$ for penalizing the elastic stiffness matrix and $q = 0.5$ for the mass matrix. Optimal design obtained by J. Du and N. Olhoff [29] is shown in Figure 5.6(d).

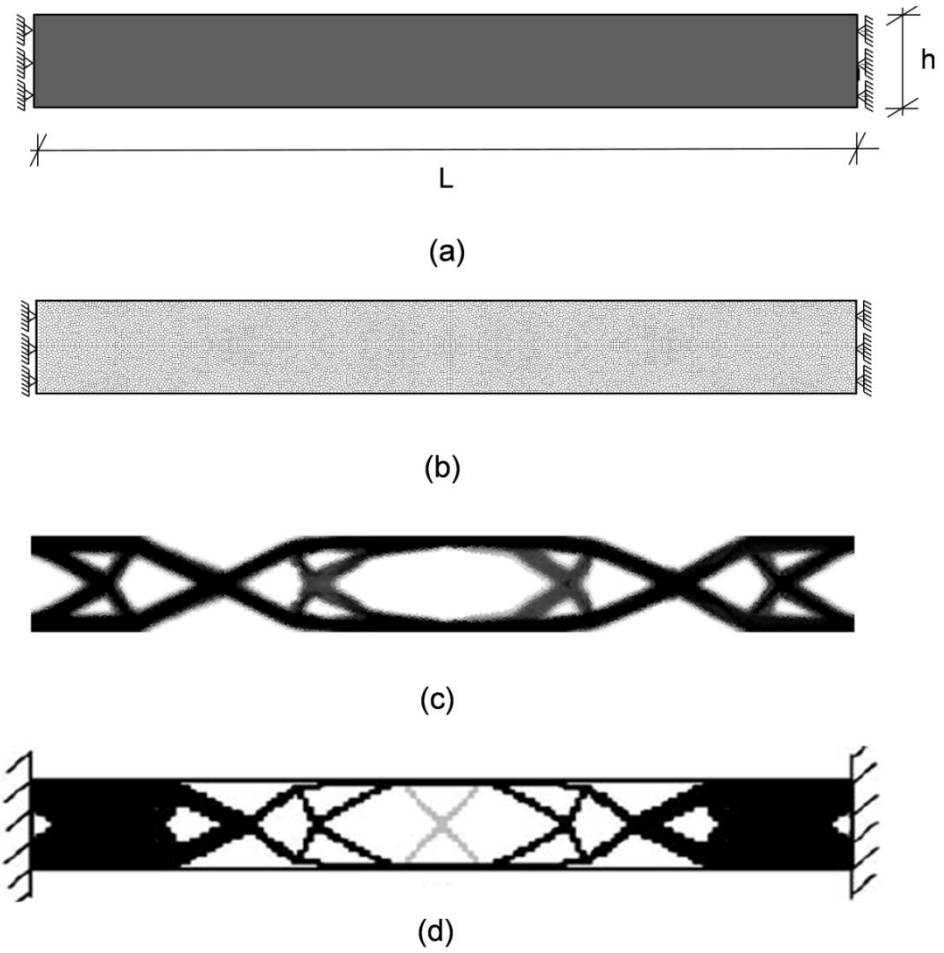

Figure 5.6: Clamped-clamped beam: (a) Geometry and boundary conditions; (b) Polygonal finite element mesh; (c) Optimal topology and (d) Optimal topology obtained by [29]**.**

Figure 5.7(a) illustrates the convergence of the objective function (*i.e.* the the fundamental eigenfrequency) and the next two eigenfrequencies with respect to the number of iterations. Figure 5.7(b) shows the results obtained by J. Du and N. Olhoff [29].

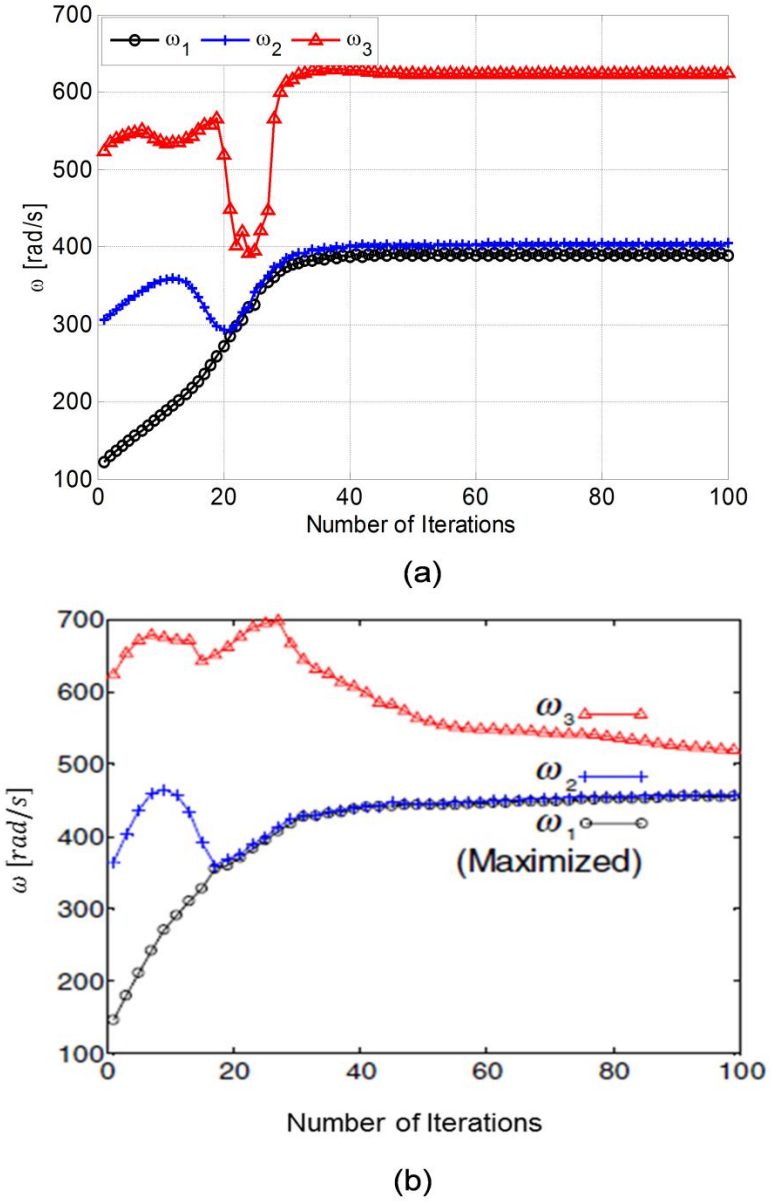

Figure 5.7: Clamped-clamped beam: (a) Convergence of the first three eigenfrequencies ; (b) Results obtained by [29].

Finally, Figure 5.8(a) shows the optimal topology obtained when the second eigenfrequency is maximized, considering the clamped-clamped case and polygonal finite elements. Figure 5.8(b) shows the final topology obtained by J. Du and N. Olhoff [29].

(a)

(b)

Figure 5.8: Clamped-clamped beam: (a) Optimal topology for maximizing the second eigenfrequency (b) Results obtained by [29].

5.1.3
Clamped Supported Beam

Figure 5.9(a) and Figure 5.9(b) show, respectively, a clamped–supported beam and the corresponding polygonal finite element mesh. The final topology obtained for maximizing the fundamental eigenfrequency is illustrated in Figure 5.9(c). We adopted $p = 6$ for penalizing the elastic stiffness matrix and $q = 0.5$ for the mass matrix. Optimal design obtained by J. Du and N. Olhoff [29] is shown in Figure 5.9(d).

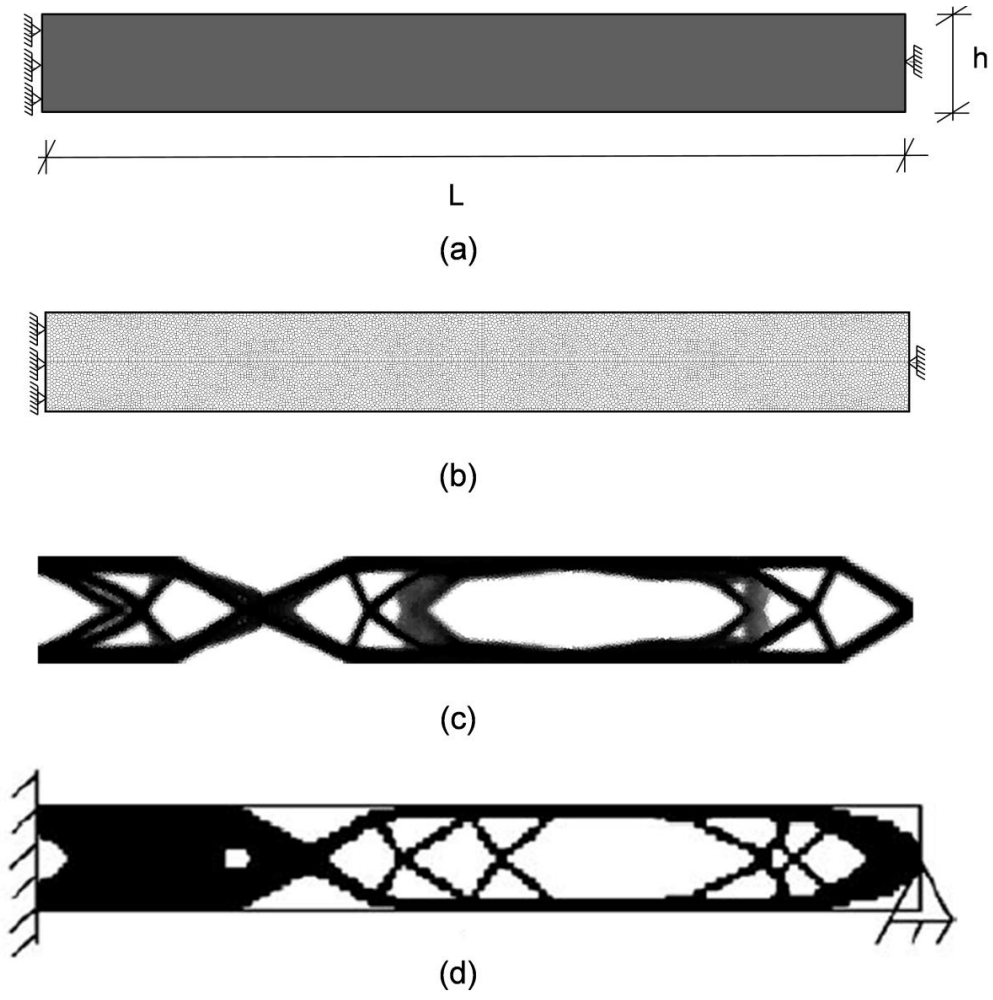

Figure 5.9: Clamped-supported beam: (a) Geometry and boundary conditions; (b) Polygonal finite element mesh; (c) Optimal topology; and (d) Optimal topology obtained by [29].

Figure 5.10(a) illustrates the convergence of the objective function (*i.e.* the fundamental eigenfrequency) and the next two eigenfrequencies with respect to

the number of iterations. Figure 5.10(b) shows the results obtained by J. Du and N. Olhoff [29].

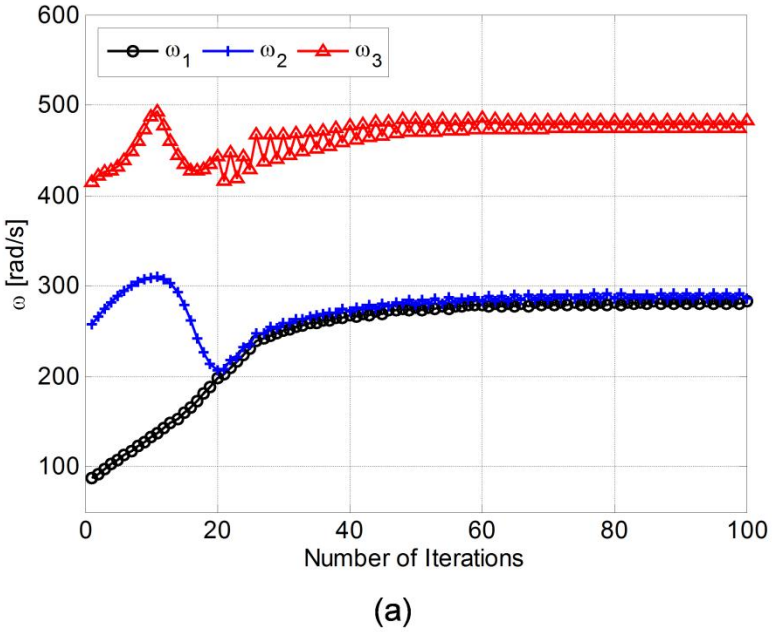

(a)

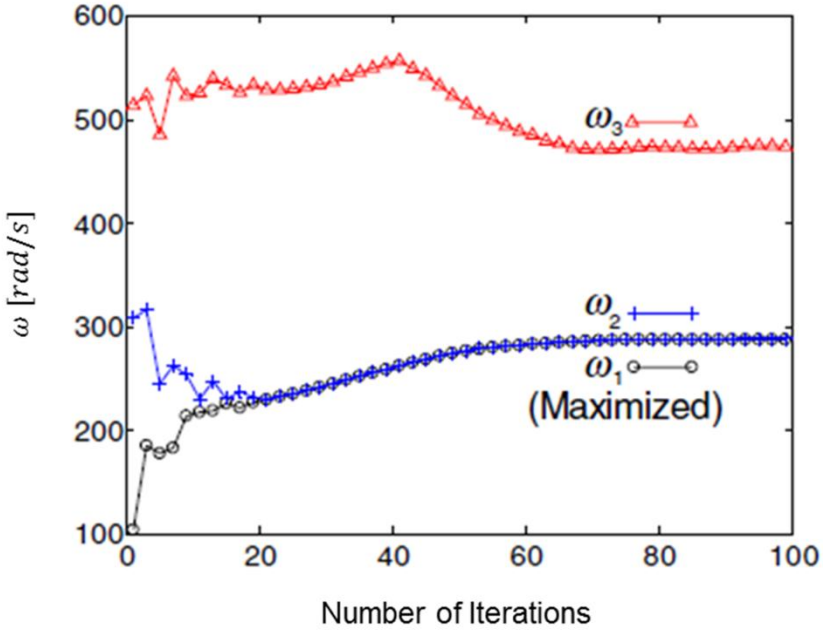

(b)

Figure 5.10: Clamped-supported beam: (a) Convergence of the first three eigenfrequencies; (b) Results obtained by [29].

Finally, Figure 5.11(a) shows the optimal topology obtained when the second eigenfrequency is maximized, considering the clamped-supported case

and polygonal finite elements. Figure 5.11(b) shows the final topology obtained by J. Du and N. Olhoff [29].

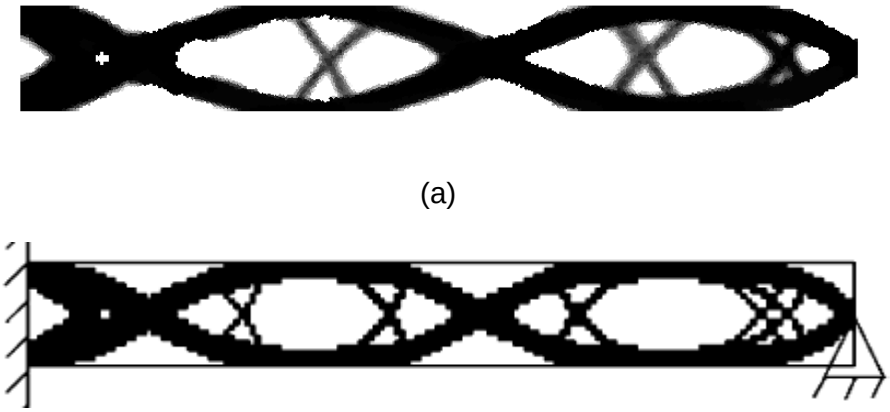

(a)

(b)

Figure 5.11: Clamped-supported beam: Optimal topology for maximizing the second eigenfrequency;(a) Present study; (b) Results obtained by [29].

Table 5.1 summarizes the results obtained for maximizing the fundamental eigenfrequency ($\omega_{1_{max}}$) and also for maximizing the second eigenfrequency ($\omega_{2_{max}}$), for the various types of boundary conditions: *S – S* (simply–supported), *C – C* (clamped–clamped), and *C – S* (clamped–supported). The results are compared to the ones obtained by J. Du and N. Olhoff [29].

Table 5.1: Maximum values of first and second eigenfrequencies.

	Present work			Reference [29]		
(rad/s)	*S – S*	*C – C*	*C – S*	*S – S*	*C – C*	*C – S*
$\omega_{1_{max}}$	*194.20*	*389.00*	*283.00*	*174.70*	*456.40*	*288.70*
$\omega_{2_{max}}$	*453.56*	*662.99*	*596.51*	*598.30*	*849.00*	*732.80*

5.2.
Topology optimization for buckling problems

This example consists of a slender column that has a unit thickness modeled with 3000 polygonal finite elements. The main input parameters are $L = 4\,m$, $h = 1\,m$, the Young's modulus E and Poisson's ratio υ are $10^7\ N/m^2$ and 0.3, respectively. $P = 0.5\,N$ is applied on the top corners, as illustrated in Figure 5.12(a). For the optimization process, we use a filter with radius $r_{min} = 0.09$, penalization factor $p = 7$ for the elastic stiffness matrix, and $g = 3$ for the geometric stiffness matrix. The Ersatz parameter $eps = 10^{-4}$, volume fraction is 65%, and the total number of iterations is 200.

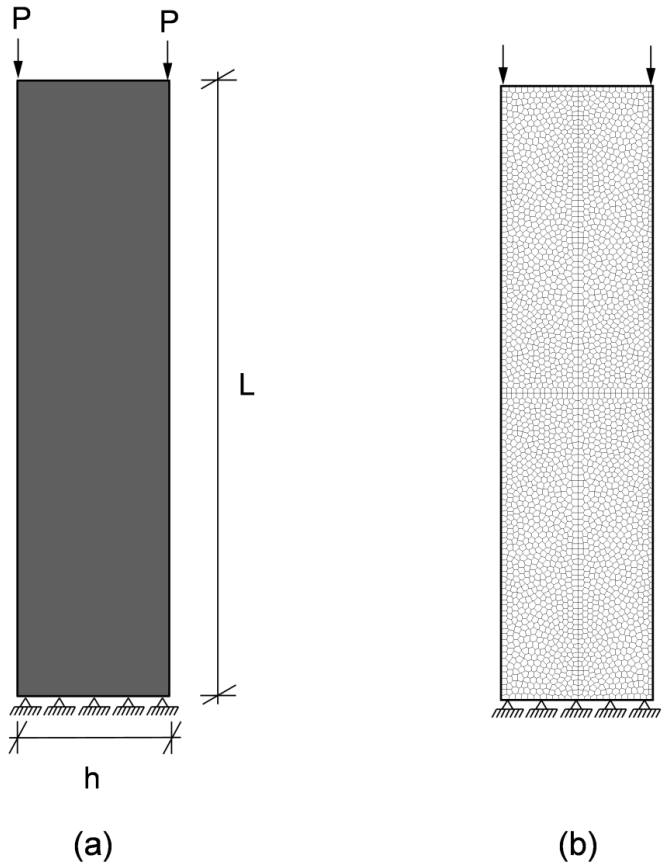

Figure 5.12: Slender column subjected to a compression load: (a) Geometry and boundary conditions considered; (b) Polygonal finite element mesh.

Figure 5.13 shows the optimal topology obtained for the buckling problem. As shown, the results are in good agreement with the ones obtained by M. P. Bendsøe and O. Sigmund [11].

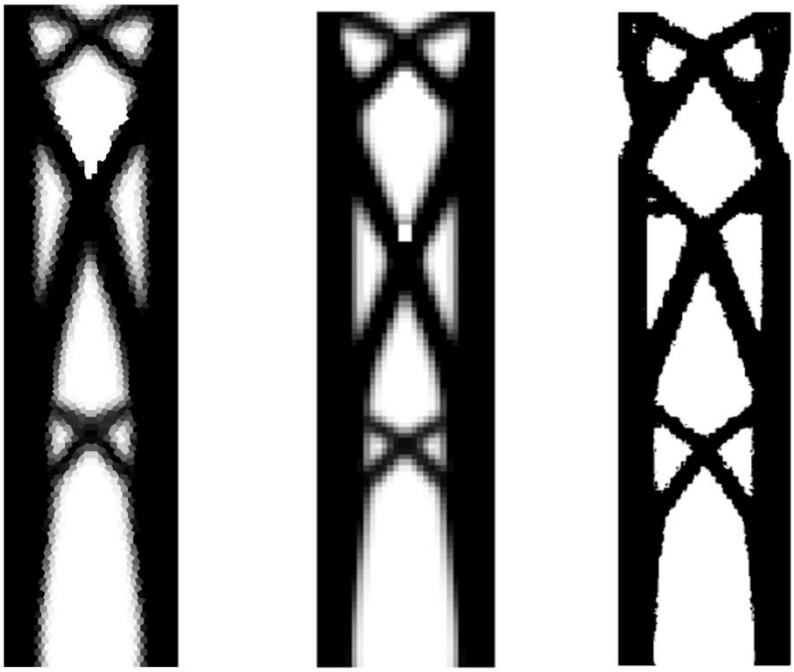

Figure 5.13: Optimal topology for maximizing the first eigenvalue (a) Using polygons (present study) ;(b) Using quads (present study) ;(c) Results obtained by [14].

Figure 5.14 illustrates the convergence of the objective function (*i.e.* the first eigenvalue) with respect to the number of iterations, using polygonal meshes. Notice that the value of the critical load in the first iteration is $P_{crit} = 1.0544 \times 10^4$ and the maximum value of the critical load (obtained after 200 iterations) is $P_{crit} = 4.2841 \times 10^4$. Figure 5.15 shows the convergence of the objective function and the first five eigenvalues.

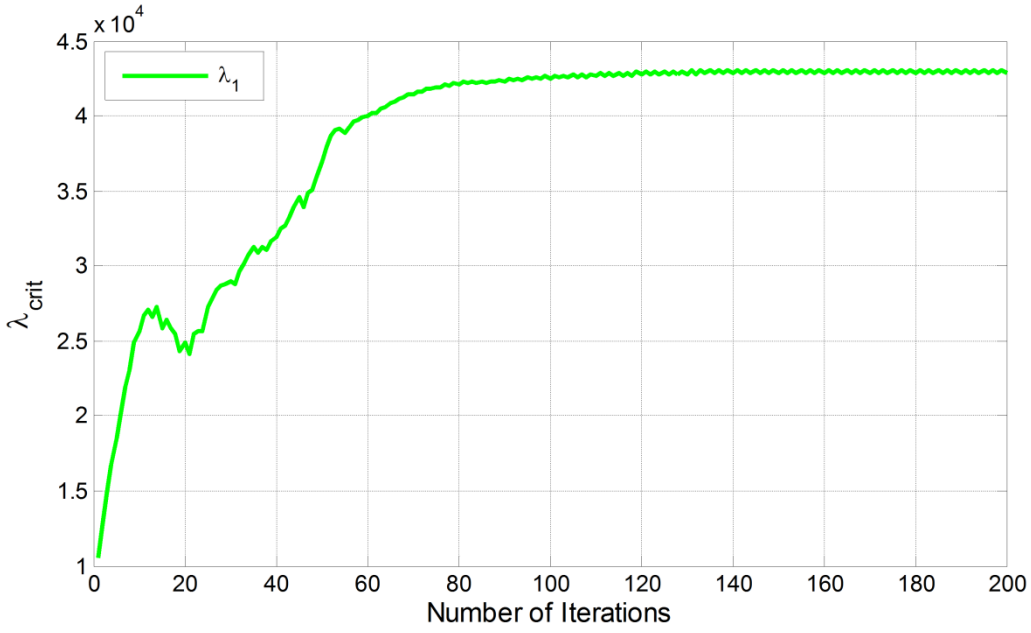

Figure 5.14: Convergence of the first eigenvalue using polygonal meshes.

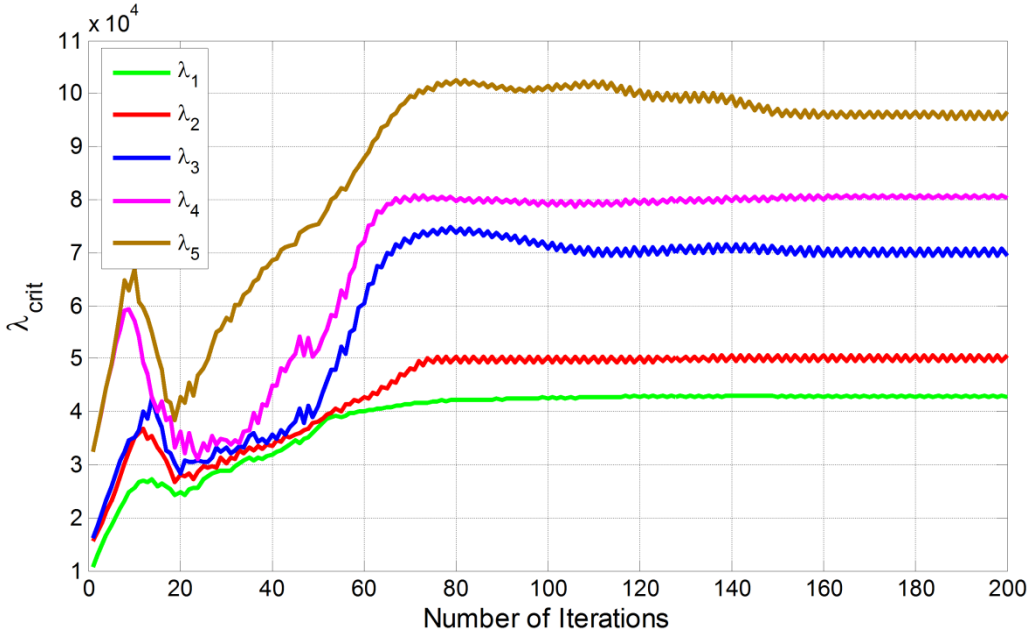

Figure 5.15: Convergence of the first five eigenvalues using polygonal meshes.

Finally, Figure 5.16 illustrates the deformed shape, first mode shape (with $P\_crit_1 = 4.2841 \times 10^4$), and second mode shape (with $P_{crit2} = 5.0592 \times 10^4$) after 200 iterations of the topology optimization process.

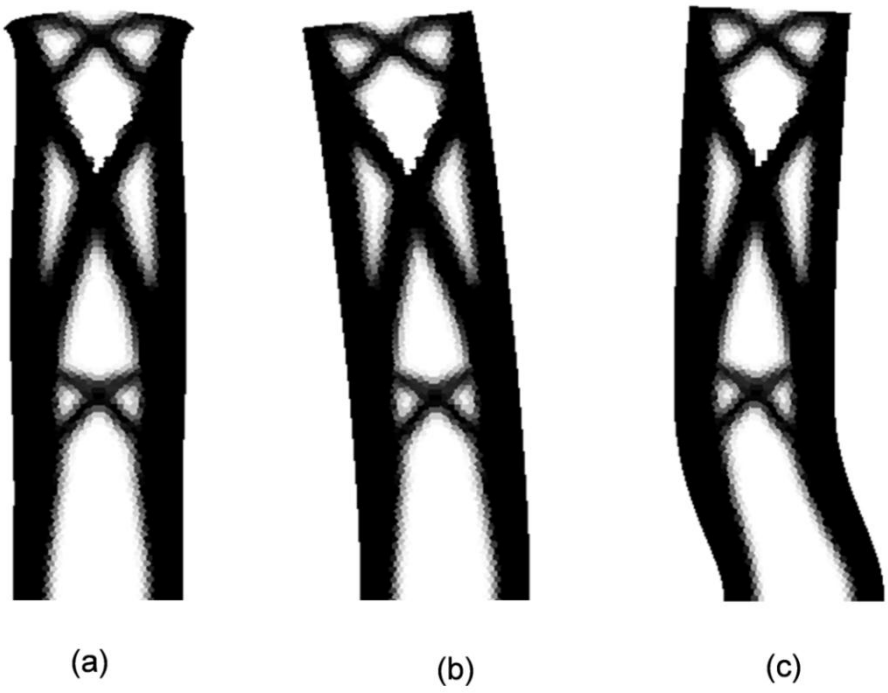

Figure 5.16: Optimal topology obtained after 200 iterations, maximizing the first eigenvalue, using polygonal elements: (a) Deformed shape after convergence; (b) First mode shape; (c) Second mode shape.

6.
Conclusions and Extensions

6.1.
Concluding Remarks

In this work we presented a study of topology optimization applied to eigenvalue problems, such as the maximization of a natural frequency or a linearized buckling load, using polygonal finite element meshes in arbitrary two-dimensional domains.

Because we used gradient methods to optimize the structures, the sensitivities of the objective and constraint functions were very important. We discussed three sensitivity approaches, namely the FDM, the DDM, and the AM. The computational cost of each method depends on the number of times that the associated linear system of equations needs to be solved. While the DDM requires a solution of a linear system of equations for each design variable, the AM requires a solution of a linear system of equations for each output function of the problem. Therefore, the AM is shown to be the most efficient method for computing sensitivities, because in our case, the optimization problem is formulated with only one output function (*i.e.*, a natural frequency or a buckling load) regardless of the number of design variables used. Note that the FDM is only used here for comparison purposes because of its well-known high computational cost. A typical problem that arises when we apply topology optimization to buckling problems is the appearance of low-density regions during the optimization process, which may generate spurious buckling modes. We addressed this problem by implementing a strategy that is based on the use of different penalization factors (for the elastic and geometric stiffness matrices). Finally, we presented several representative examples that demonstrated the robustness and efficiency of the proposed framework for topology optimization applied to both eigenfrequency and buckling problems.

6.2.
Suggestions for Future Work

The main suggestions for future research in this area are:

- Extend the proposed framework to different structures such as plates and shells;
- Investigate a typical problem, known as multiplicity of eigenvalues, which may appear when topology optimization is applied to eigenvalue problems. During the optimization process, it can be observed that while the first eigenvalue is increasing, the subsequent eigenvalues are decreasing, and gradually, the first two or more eigenvalues may converge to the same value although the corresponding eingenvectors may remain different;
- We also propose to further investigate another typical problem, namely mode switching, which is usually observed when applying topology optimization to maximize the buckling load;
- Consider stress constraints in the formulation of the topology optimization problem to avoid stress concentrations in the final topology;
- Finally, with respect to the CPU time for computing the eigenvalue sensitivities, we propose to investigate a parallel topology optimization method to solve large-scale structural eigenvalue problems.

7.
Bibliography

[1] Christensen P.W. e Klarbring A., **An Introduction to Structural Optimization**, vol. 153.,pages 214, 2009, ISBN 978-1-4020-8665-6 e-ISBN 978-1-4020-8666-3

[2] Olason A. e Tidman D., **Methodology for Topology and Shape Optimization in the Design Process**, Masters Dissertation, Chalmers University of Technology, Goteberg, Sweden, 2010.

[3] Valencia C. A. M., **Topology optimization in the design of mechanical structural elements**, (in spanish), Thesis, Universidad Autónoma de Occidente, 2012.

[4] Stromberg L. L., Beghini A., Baker W. F., e Paulino G. H., Topology optimization for braced frames: Combining continuum and beam/column elements, ***Eng. Struct.***, vol. 37, p. 106–124, 2012.

[5] Talischi C., Paulino G. H., Pereira A., e Menezes I. F. M., Polygonal finite elements for topology optimization: A unifying paradigm, ***Int. J. Numer. Methods Enginnering***, n^{o} August, p. 1885–1891, 2009.

[6] Browne P. A., **Topology Optimization of Linear Elastic Structures**, Doctoral Thesis, University of Bath, 2013.

[7] Pereira A., Talischi C., Menezes I. F. M., e Paulino G. H., Checkerboard-Free Topology Optimization Using Polygonal Finite Elements, ***Asoc. Argentina Mecánica Comput.***, vol. XXIX, p. 15–18, 2010.

[8] Talischi C., Paulino G. H., Pereira A., e Menezes I. F. M., PolyMesher: a general-purpose mesh generator for polygonal elements written in Matlab, ***Struct. Multidiscip. Optim.***, vol. 45, n^{o} 3, p. 309–328, 2012.

[9] Talischi C., Pereira A., Paulino G. H., e Menezes I. F. M., Polygonal finite elements for incompressible fluid flow, ***Int. J. Numer. Methods Fluids***, n^{o} October 2007, p. 601–629, 2013.

[10] Tacoma Narrows Brigde, 2015. [Online]. Available at: https://es.wikipedia.org/wiki/Puente_de_Tacoma_Narrows#/media/File:Tacoma_Narrows_Bridge-3.jpg. (Document), [Acessado: 26-nov-2015].

[11] OM Ingenieria Obras Metálicas, 2015. [Online]. Available at: http://www.omingenieria.com/portafolio.php?p=portafolio&pagina=2., (Document), [Acessado: 26-nov-2015].

[12] Altair Techonology Conference, Topology optimization of Nose and Forward Fuselage, 2015. [Online]. Available at: http://www.altairatc.com/presentations/europe/2015/day-3/steliaaero_kawski.aspx., (Document), [Acessado: 22-jan-2016].

[13] Evgueni F., Junho C., Paulino G. H., e Junho S., Polygonal Multiresolution Topology Optimization (PolyMtop) for Structural Dynamics, ***Struct. Multidiscip. Optim.***, p. 1–22, 2014.

[14] Bendsøe M. P. e Sigmund O., Topology optimization: theory, methods, and applications, vol. 2nd Editio, nº 724. 2003.

[15] Neves M.M., Rodrigues H., e Guedes J. M., Generalized Topology design of Structures with a buckling load criterion, ***Struct. Optim.***, vol. 78, p. 71–78, 1995.

[16] Rodrigues H. C., Guedes J. M., e Bendsøe M. P., Necessary conditions for optimal design of structures with a nonsmooth eigenvalue based criterion, ***Struct. Optim.***, vol. 9, nº 1, p. 52–56, fev. 1995.

[17] Lund E., Buckling topology optimization of laminated multi-material composite shell structures, ***Compos. Struct.***, vol. 91, nº 2, p. 158–167, 2009.

[18] Van den Boom S. J., **Topology Optimisation Including Buckling Analysis**, Masters Dissertation, Delf University of Technology, 2014.

[19] Luo Q. e Tong L., Structural topology optimization for maximum linear buckling loads by using a moving iso-surface threshold method, ***Struct. Multidiscip. Optim.***, vol. 52, nº 1, p. 71–90, 2015.

[20] Gao X. e Ma H., Topology optimization of continuum structures under buckling constraints, ***Proc. - 2009 Int. Conf. Inf. Technol. Comput. Sci. ITCS 2009***, vol. 2, p. 417–420, 2015.

[21] Kim T. S., Kim J. E., e Kim Y. Y., Parallelized structural topology optimization for eigenvalue problems, ***Int. J. Solids Struct.***, vol. 41, nº 9–10, p. 2623–2641, 2004.

[22] Bratus A. S. e Seiranian A. P., Bimodal Solution in Eigenvalue Optimization Problems, ***J. Appl. Math. Mech.***, vol. 47, nº 4, p. 451–457, 1984.

[23] Seiranyan A. P., Multiple Eingenvalues in Optimization Problems, ***J. Appl. Math. Mech.***, vol. 51, nº 2, p. 349–352, 1987.

[24] Ma Z.-D., Cheng H.-C., e Kikuchi N., Structural design for obtaining desired eigenfrequencies by using the topology and shape optimization method, ***Comput. Syst. Eng.***, vol. 5, nº 1, p. 77–89, 1994.

[25] Ma Z.-D., Kikuchi N., e Cheng H.-C., Topological design for vibrating structures, ***Comput. Methods Appl. Mech. Eng.***, vol. 121, nº 94, p. 259–280, 1995.

[26] Xie Y. M. e Steven G. P., Evolutionary structural optimization for dynamic problems, ***Comput. Struct.***, vol. 58, nº 6, p. 1067–1073, 1996.

[27] Huang X., Zuo Z. H., e Xie Y. M., Evolutionary topological optimization of vibrating continuum structures for natural frequencies, ***Comput. Struct***., vol. 88, nº 5–6, p. 357–364, 2010.

[28] Olhoff N. e Du J., Topology optimization of structures against vibration and noise, … ***12th Int. Congr. Sound Vib.*** …, p. 1–20, 2005.

[29] Du J. e Olhoff N., Topological design of freely vibrating continuum structures for maximum values of simple and multiple eigenfrequencies and frequency gaps, ***Struct. Multidiscip. Optim.***, vol. 34, nº 2, p. 91–110, 2007.

[30] Yoon G. H., Maximizing the fundamental eigenfrequency of geometrically nonlinear structures by topology optimization based on element connectivity parameterization, ***Comput. Struct.***, vol. 88, nº 1–2, p. 120–133, 2010.

[31] Olhoff N., Niu B., e Cheng G., Optimum design of band-gap beam structures, ***Int. J. Solids Struct.***, vol. 49, nº 22, p. 3158–3169, 2012.

[32] Talischi C., Paulino G. H., Pereira A., e Menezes I. F. M., PolyTop: a Matlab implementation of a general topology optimization framework using unstructured polygonal finite element meshes, ***Struct. Multidiscip. Optim.***, vol. 45, nº 3, p. 329–357, 2012.

[33] Cook R. D., Malkus D. S., Plesha M. E., e Witt R. J. W., Concepts and Applications of Finite Element Analysis,4th edition,Prentice-Hall, Madison, USA, ISBN 978-0-471-35605-9,pages 703, 2002.

[34] Bathe K. J., Finite Element Procedures in Engineering Analysis, ISBN 0-13-301458-4, New Jersey, USA: Prentice Hall, Inc., 1982.

[35] Inman D. J., Engineering Vibration, 3º ed. New Jersey, ISBN 0-13-228173-2, USA: Pearson Education, Inc., 2007.

[36] Gere J. M., Mechanics Materials, (in portuguese), vol. 53. São Paulo, Brasil: Pioneira Thomson Learning, 1989.

[37] R. C. Hibbeler, Resistance Materials, (in portuguese), 5º ed. São Paulo: Pearson Prentice Hall, 2004.

[38] Bendsøe M. P. e Sigmund O., Material interpolation schemes in topology optimization, ***Arch. Appl. Mech.***, vol. 69, nº 9–10, p. 635–654, 1999.

[39] Talischi C., **Restriction Methods for Shape and Topology Optimization**, Doctoral Thesis, University of Illinois at Urbana-Champaign, 2012.

[40] Gunwant D. e Misra A., Topology Optimization of Continuum Structures using Optimality Criterion Approach in Ansys, ***Int. J. Adv. Eng. Technol.***, vol. 5, nº 1, p. 470–485, 2012.

[41] Svanberg K., The Method of Moving Asymptotes-A new method for Structural Optimization, ***Int. J. Numer. Methods Enginnering***, vol. 24, p. 359–373, 1987.

[42] Groenwold A. A. e Etman L. F. P., On the equivalence of optimality criterion and sequential approximate optimization methods in the classical topology layout problem, ***Int. J. Numer. Methods Enginnering***, n^{o} March, p. 1885–1891, 2007.

[43] Pedersen N. L., Maximization of eigenvalues using topology optimization, ***Struct. Multidiscip. Optim.***, vol. 20, n^{o} 1, p. 2–11, 2000.

[44] Mosmann R. M., **Topology optimization of continuous structures subjected to flexibility constraints, volume and natural frequency**, (in portuguese), Masters Dissertation, Universidade Federal do Rio Grande do Sul, Brasil, 2003.

[45] Guilherme C. E. M., **Topology optimization of trusses and frames with buckling and flexibility restrictions**, (in portuguese), Masters Dissertation, Universidade Federal do Rio Grande do Sul, Brasil, 2000.